# Transport of Asian ozone pollution into surface air over the western United States in spring

Meiyun Lin,[1,2] Arlene M. Fiore,[2,3] Larry W. Horowitz,[2] Owen R. Cooper,[4,5] Vaishali Naik,[2,6] John Holloway,[5] Bryan J. Johnson,[5] Ann M. Middlebrook,[5] Samuel J. Oltmans,[4] Ilana B. Pollack,[4,5] Tomas B. Ryerson,[5] Juying X. Warner,[7] Christine Wiedinmyer,[8] John Wilson,[2] and Bruce Wyman[2]

Received 4 October 2011; revised 3 December 2011; accepted 14 December 2011; published 17 February 2012.

[1] Many prior studies clearly document episodic Asian pollution in the western U.S. free troposphere. Here, we examine the mechanisms involved in the transport of Asian pollution plumes into western U.S. surface air through an integrated analysis of in situ and satellite measurements in May–June 2010 with a new global high-resolution ($\sim$50 $\times$ 50 km$^2$) chemistry-climate model (GFDL AM3). We find that AM3 with full stratosphere-troposphere chemistry nudged to reanalysis winds successfully reproduces observed sharp ozone gradients above California, including the interleaving and mixing of Asian pollution and stratospheric air associated with complex interactions of midlatitude cyclone air streams. Asian pollution descends isentropically behind cold fronts; at $\sim$800 hPa a maximum enhancement to ozone occurs over the southwestern U.S., including the densely populated Los Angeles Basin. During strong episodes, Asian emissions can contribute 8–15 ppbv ozone in the model on days when observed daily maximum 8-h average ozone (MDA8 $O_3$) exceeds 60 ppbv. We find that in the absence of Asian anthropogenic emissions, 20% of MDA8 $O_3$ exceedances of 60 ppbv in the model would not have occurred in the southwestern USA. For a 75 ppbv threshold, that statistic increases to 53%. Our analysis indicates the potential for Asian emissions to contribute to high-$O_3$ episodes over the high-elevation western USA, with implications for attaining more stringent ozone standards in this region. We further demonstrate a proof-of-concept approach using satellite CO column measurements as a qualitative early warning indicator to forecast Asian ozone pollution events in the western U.S. with lead times of 1–3 days.

**Citation:** Lin, M., et al. (2012), Transport of Asian ozone pollution into surface air over the western United States in spring, *J. Geophys. Res.*, *117*, D00V07, doi:10.1029/2011JD016961.

## 1. Introduction

[2] Analyses of available observations indicate an increase of springtime ozone ($O_3$) mixing ratios in the free troposphere and at surface sites of the western United States since the 1980s [*Jaffe et al.*, 2003a; *Oltmans et al.*, 2008; *Parrish et al.*, 2009; *Cooper et al.*, 2010], coincident with rising Asian anthropogenic emissions of $O_3$ precursors as inferred from satellite measurements of column $NO_2$ and bottom-up inventories [*e.g. Richter et al.*, 2005; *Ohara et al.*, 2007; *Q. Zhang et al.*, 2009]. Global model simulations further support the role of rising Asian emissions in contributing to the springtime $O_3$ trend in the western U.S. [*Jacob et al.*, 1999; *Zhang et al.*, 2008]. Many prior studies clearly document episodic Asian pollution in the free troposphere over this region [*e.g. Jaffe et al.*, 1999; *Yienger et al.*, 2000; *Heald et al.*, 2003; *Jaeglé et al.*, 2003; *Cooper et al.*, 2004a; *Goldstein et al.*, 2004; *Hudman et al.*, 2004; *Zhang et al.*, 2008]. The extent to which this pollution is entrained into the boundary layer is unclear [*Brown-Steiner and Hess*, 2011] yet has implications for attainment of U.S. air quality standards. Here, we seek greater understanding of the mechanisms that transport Asian pollution

[1]Atmospheric and Oceanic Sciences, Princeton University, Princeton, New Jersey, USA.
[2]NOAA Geophysical Fluid Dynamics Laboratory, Princeton, New Jersey, USA.
[3]Now at Lamont-Doherty Earth Observatory, Columbia University, Palisades, New York, USA.
[4]Cooperative Institute for Research in Environmental Sciences, University of Colorado at Boulder, Boulder, Colorado, USA.
[5]NOAA Earth System Research Laboratory, Boulder, Colorado, USA.
[6]High Performance Technologies, Inc., NOAA Geophysical Fluid Dynamics Laboratory, Princeton, New Jersey, USA.
[7]Joint Center for Earth Systems Technology, University of Maryland, Baltimore County, Baltimore, Maryland, USA.
[8]National Center for Atmospheric Research, Boulder, Colorado, USA.


0148-0227/12/2011JD016961

into western U.S. surface air through an integrated analysis of in situ and satellite measurements with a new high-resolution ($\sim 50 \times 50$ km$^2$) global chemistry-climate model (GFDL AM3) [*Donner et al.*, 2011]. In particular, we quantify the contribution of Asian pollution to surface $O_3$ levels on highly polluted days in both densely populated regions such as the Los Angeles (LA) Basin and in rural areas such as national parks.

[3] The threshold value for the U.S. primary National Ambient Air Quality Standard (NAAQS) for ground-level $O_3$, based on the 4th highest daily maximum 8-h concentration (MDA8) averaged over three years, has been lowered twice since the 1980s, with the current 75 ppbv threshold implemented in May 2008. In 2010, the U.S. EPA proposed to further revise the NAAQS $O_3$ threshold to one in the range of 60–70 ppbv [*Environmental Protection Agency*, 2010]. If a 60 ppb threshold were to be adopted, the number of violating counties across the USA would double (based on the 2006–2008 monitoring data, http://www.epa.gov/air/ozonepollution/pdfs/20100104maps.pdf). The rising Asian contribution to U.S. surface $O_3$ levels poses an additional challenge to meeting more stringent NAAQS for $O_3$ [*Lefohn et al.*, 1998; *Fiore et al.*, 2002; *Keating et al.*, 2004]. Earlier work indicates that the contribution of Asian emissions to surface $O_3$ in the U.S. reflects mostly an enhancement in background levels [e.g., *Goldstein et al.*, 2004; *Zhang et al.*, 2008], and generally decreases on highly polluted days in summer [e.g., *Fiore et al.*, 2002]. However, a few recent studies suggest a correlation between $O_3$ entering the U.S. west coast and local pollution episodes in California [e.g., *Parrish et al.*, 2010; *Huang et al.*, 2010; *Pfister et al.*, 2011]. At present, quantitative estimates of the specific sources of $O_3$ flowing into the western USA (e.g., recirculation of North American emissions, intercontinental transport, stratosphere-to-troposphere exchange, and other natural sources) are lacking. Advancing our understanding of the contribution from these sources to total surface $O_3$ over the western U.S. is crucial to inform the NAAQS-setting process and to develop effective state implementation plans (SIPs; the process by which states demonstrate their path to achieving compliance with the NAAQS; http://www.epa.gov/air/urbanair/sipstatus/).

[4] Pollution transported from Asia to North America originates in the boundary layer of East Asia, where primary air pollutants are directly emitted from combustion and industrial sources. The polluted air masses are exported from the Asian boundary layer to the free troposphere via large-scale lifting such as deep convection or warm conveyor belts embedded in midlatitude cyclones [e.g., *Carmichael et al.*, 2003; *Liu et al.*, 2003; *Cooper et al.*, 2004a; *Ding et al.*, 2009; *Lin et al.*, 2010] as well as via mesoscale processes such as orographic forcing and mountain-chimney effects [e.g., *Chen et al.*, 2009]. The exported pollutants traverse the North Pacific Ocean in the mid- and upper troposphere, and eventually descend toward the surface [e.g., *Task Force on Hemispheric Transport of Air Pollution* (*TFHTAP*), 2011; *Brown-Steiner and Hess*, 2011, and references therein]. Observational studies document the frequent transport of Asian dust, sulfate aerosol and mercury to the surface of western North America, and on rare occasions these events can be relatively strong [*Husar et al.*, 2001; *Jaffe et al.*, 2003b; *McKendry et al.* 2008; *Weiss-Penzias et al.* 2007; *Ewing et al.* 2010]. While these events are common, modeling studies suggest that only a small portion (<10%) of the Asian pollutants reaching the North American free troposphere actually descends into surface air [*Yienger et al.*, 2000; *Cooper et al.*, 2004a; *L. Zhang et al.*, 2009]. However, these prior estimates, based on global-scale chemical transport models (CTMs) or Lagrangian trajectory models, both driven with meteorological fields typically at $2° \times 2°$ horizontal resolution, may be conservative as these coarse-resolution models have limitations in capturing meso-scale processes contributing to the exchange of pollutants between the boundary layer and the free troposphere. The dilution of intense plumes due to numerical diffusion in global-scale models further diminishes the modeled impacts of vigorous episodic transport events [e.g., *Lin et al.*, 2010; *Rastigejev et al.*, 2010, and references therein].

[5] An additional goal of this study is to extend earlier efforts that developed meteorological indices to characterize the daily to interannual strength of Asian pollution outflow and trans-Pacific transport [*Liu et al.*, 2005, *Liang et al.*, 2005]. We hypothesize that space-based instruments are useful for developing these indices given their vast spatial coverage at near-daily intervals and their ability to capture variability in chemical composition associated with synoptic-scale weather patterns. Over the last decade, satellite remote sensing has been widely used to advance our understanding of large-scale outflow of carbon monoxide (CO) from major biomass-burning regions [e.g., *Edwards et al.*, 2003; *McMillan et al.*, 2005, 2008], pollution transport to the Arctic [e.g., *Stohl et al.*, 2007], intercontinental transport of air pollution [e.g., *Heald et al.*, 2003; *Zhang et al.*, 2008; *Pfister et al.*, 2011], and natural dust [e.g., *Chin et al.*, 2007; *Uno et al.*, 2009; *Li et al.*, 2010]. Specifically, we explore the potential for near real-time space-based measurements of CO columns to help inform regional air quality management decisions regarding the potential for Asian pollution to enhance surface $O_3$ concentrations over the western USA.

[6] Section 2 briefly describes the model simulations and observational data. We focus our analysis on May–June 2010, leveraging intensive in situ vertical profiling of $O_3$ and related species during the NOAA CalNex (Research at the Nexus of Air Quality and Climate Change) field campaign in California (http://www.esrl.noaa.gov/csd/calnex). Section 3 examines the transport pathways of Asian pollution over the western U.S., including the influence of midlatitude cyclones, mixing of Asian polluted air masses with stratospheric air, and isentropic transport mechanisms. We then summarize the model evaluation (section 4) and the average impacts of Asian anthropogenic emissions on U.S. surface $O_3$, including the contribution to high-$O_3$ events during the CalNex period (section 5). Section 6 illustrates a proof-of-concept approach developing a space-based index to identify situations under which episodic Asian pollution plumes may affect surface $O_3$ air quality over the western USA.

## 2. Measurements and Model

### 2.1. Meteorological and Chemical Environment in May–June 2010

[7] The Asian contribution to $O_3$ in the western U.S. is determined by the amount of $O_3$ produced in the Asian

boundary layer, by the strength and position of the North Pacific storm track, and by additional $O_3$ produced during transport. May–June is the beginning of the $O_3$ pollution season at northern midlatitudes, with the East Asian coast experiencing maximum $O_3$ concentrations prior to the onset of the East Asian summer monsoon [e.g., *Tanimoto et al.*, 2005; *Lin et al.*, 2009]. The ridge-trough pattern over the eastern North Pacific and western U.S. was amplified during May–June 2010, resulting in stronger surface anticyclones and northwesterly surface winds relative to climatology [*Cooper et al.*, 2011]. According to the NOAA Climate Prediction Center (http://www.cpc.ncep.noaa.gov), the 2009–2010 winter was influenced by strong El Niño conditions. *Koumoutsaris et al.* [2008] show that springtime Asian pollution outflow may be enhanced following an El Niño winter due to changes in convective activity in East Asia as well as the strengthening and southeastward extension of the North Pacific storm track. We therefore expect that meteorological conditions during May–June 2010 led to a particularly active season for export of Asian pollution and its subsequent transport to the southwestern U.S. These conditions, in conjunction with the suite of observations collected during the CalNex campaign (section 2.2), offer an invaluable opportunity to improve our mechanistic understanding of Asian pollution transport.

### 2.2. In Situ Measurements

[8] During the CalNex campaign, near-daily ozonesondes were launched at six sites in California (Figure S1 in the auxiliary material) between May 10 and June 19, 2010, to measure baseline $O_3$ at the U.S. west coast [*Cooper et al.*, 2011].[1] For comparison with these measurements, we sample AM3 at the location and times of sonde launches, interpolate to the sonde pressure, and then average both the measured and model values over 0.5 km altitude bins. Three-hourly model fields are used, linearly interpolated to the sonde launch times (14:00–16:59 Pacific Daylight Time). We also use collocated measurements of $O_3$, $NO_x$, $NO_y$, CO, sulfate and organic aerosols aboard the NOAA WP-3D aircraft during CalNex to characterize Asian pollution layers above California (section 3.3) and to evaluate the model (section 4). Measurement techniques are described in prior publications [*Ryerson et al.*, 1998; *Holloway et al.*, 2000; *Drewnick et al.*, 2005; *Bahreini et al.*, 2009]. For ground-level $O_3$, we compare daily maximum 8-h average $O_3$ (hereafter MDA8 $O_3$) sampled at the model surface layer with observations from the U.S. EPA's Clean Air Status and Trends Network (CASTNet) and Air Quality System (AQS) database. For all model comparisons to in situ measurements, we apply a bilinear interpolation technique, obtaining the value at the sample location as a quadratic function of model results at the nearest four grid cells.

### 2.3. Satellite Data

[9] We use observations of CO and $O_3$ total column amounts from the Atmospheric Infrared Sounder (AIRS) onboard the NASA Aqua satellite to identify trans-Pacific Asian pollution events and stratospheric $O_3$ intrusions, respectively. The AIRS cross-track scanning grating spectrometer coupled with the Aqua cross-track scanning Advanced Microwave Sounding Unit (AMSU) provides vertical profiles of the atmosphere with a nadir 45 km field of regard (FOR) across a 1650 km swath [*Aumann et al.*, 2003]. The broad swath, infrared spectral coverage, and reconstructed cloudy pixels [*Susskind et al.*, 2003] of AIRS enable retrievals over nearly 70% of the planet every day with substantial portions of the globe observed twice daily (ascending and descending orbits), thus providing a unique opportunity for process studies of synoptic-scale chemical transport in the global atmosphere [*McMillan et al.*, 2005, 2008]. In this study we use version 5.2 Level 3 daily $1° \times 1°$ gridded standard products (AIRX3STD) of AIRS CO [*McMillan et al.*, 2011] and $O_3$ total column retrievals [*Susskind et al.*, 2003], downloaded from the NASA Goddard Earth Sciences Data and Information Services Center (http://disc.sci.gsfc.nasa.gov/). The ascending and descending retrievals are averaged to minimize the day-night difference and to provide better spatial coverage.

[10] The main sensitivity of AIRS to tropospheric CO occurs between approximately 300 and 600 hPa with a typical Degrees Of Freedom for Signals (DOFS) at northern midlatitudes of approximately 1 [*Warner et al.*, 2007, 2010]. AIRS V5 CO retrievals are biased high by 6–10% between 900 and 300 hPa in the northern midlatitudes with a root-mean square error of 8–12% [*McMillan et al.*, 2011]. A number of validation exercises reveal that AIRS $O_3$ profile retrievals capture the large-scale dynamic variability and gradients of $O_3$ in the extratropical UT/LS region [e.g., *Pan et al.*, 2007; *Pittman et al.*, 2009; *Wei et al.*, 2010].

### 2.4. GFDL AM3 Model Simulations

[11] AM3 is the atmospheric component of the GFDL global coupled atmosphere-oceans-land-sea ice model (CM3) [*Donner et al.*, 2011; *Griffies et al.*, 2011]. The AM3 cubed-sphere grid greatly improves polar representation and computational efficiency [*Putman and Lin*, 2007]; the model's horizontal resolution is denoted as Cn, where n is an integer number indicating total number of cells (finite volumes) along each edge of the cube. We apply C180 (where the size of the grid cell varies from 43 km at the 6 corners of the cubed sphere to 62 km near the center of each face) and C48 (163–231 km) horizontal resolution. Model simulations at the C48 resolution starting in January 2009 were used to initialize the C180 simulations spanning January–June 2010. Both coarse- and high-resolution simulations employ the same physical parameterizations and include 48 vertical levels, ranging in thickness from 70 m near the Earth's surface to 1–1.5 km near the tropopause and 2–3 km in much of the stratosphere.

[12] AM3 includes a fully coupled stratosphere-troposphere-aerosol chemistry within a general circulation model. The chemistry models of *Horowitz et al.* [2003] for the troposphere and *Austin and Wilson* [2006] for the stratosphere are merged, with updates in isoprene nitrate chemistry [*Horowitz et al.*, 2007], chlorine and bromine chemistry [*Austin and Wilson*, 2010], gas-phase reaction rates, dry deposition velocities and heterogeneous reactions as described by *Donner et al.* [2011]. The unique feature of full stratospheric and tropospheric chemistry distinguishes the GFDL AM3 model from most current generation global and regional tropospheric CTMs, and enables a process-oriented

[1] Auxiliary materials are available in the HTML. doi:10.1029/2011JD016961.

analysis for the intermingling of Asian pollution with stratospheric air over the U.S. west coast (section 3.1). We implement a stratospheric $O_3$ tracer by defining $O_3$ above the WMO thermal tropopause each model time step as "stratospheric" ($O_3$-strat), with its transport into the troposphere driven by dynamic processes (such as tropopause folds and cut-off lows). Once mixed into tropospheric air, $O_3$-strat is subject to transport and loss (chemical and depositional) in the same manner as $O_3$ of tropospheric origin. This technique likely overestimates the stratospheric contribution since any $O_3$ above the thermal tropopause is instantly labeled as "stratospheric" regardless of its actual origin.

[13] AM3 is typically run in the climate mode, forced with prescribed sea surface temperatures (SSTs) and sea ice [e.g., *Austin and Wilson* 2010; *Golaz et al.*, 2011; *Fang et al.*, 2011; *Rasmussen et al.*, 2011] or as a component in the GFDL coupled model CM3 [*Griffies et al.*, 2011]. To enable direct comparisons with CalNex observations, AM3 simulations at both C48 and C180 horizontal resolution in this study are forced with observed SSTs as in the standard climate simulations, but horizontal winds are nudged to those from the NCEP Global Forecasting System (GFS) at T85 horizontal resolution (approximately 1.4° × 1.4°, 64 sigma levels, archived 3 hourly) [*Kanamitsu et al.*, 1991]. Our goal is to preserve the large-scale features of the observed airflow while allowing AM3 to simulate meso-scale patterns, similar to the approach taken for high-resolution regional weather forecasting [e.g., *Skamarock et al.*, 2008; *Lin et al.*, 2009, 2010] and hurricane modeling [*Knutson et al.*, 2008]. In order to minimize the impacts of noise introduced via nudging, which has been shown to lead to excessive stratosphere-to-troposphere $O_3$ transport [*van Noije et al.*, 2004, and references therein], we implemented a pressure-dependent nudging technique, relaxing the model to GFS U and V with a time scale of 6 h in the surface level, but weakening the nudging strength with decreasing pressure (e.g., relaxing with a time scale of ∼60 h by 100 hPa and ∼600 h by 10 hPa). No nudging is implemented above ∼10 hPa since the GFS model top (∼0.32 hPa) is lower than that of AM3 (∼0.01 hPa).

[14] The impact of Asian emissions is determined as the difference between a base simulation with all emissions included, and a sensitivity simulation with the East Asian (15°–50°N, 95°–160°E) anthropogenic emissions (including aerosol) shut off in the model. Methane is set to observed values (1767 ppbv) as a lower boundary condition in both simulations. The sensitivity simulation begins in January 2009 with the C48 horizontal resolution, allowing for a one-year spin-up period sufficient to capture changes in the background atmospheric composition due to Asian emissions. Horizontal winds in the sensitivity simulation are also nudged to the GFS winds, thus we expect that the large-scale transport should be similar between the two simulations although completely removing Asian emissions may induce some feedbacks on hydrological processes (particularly through aerosol-cloud interactions which are included in AM3). Further, the $O_3$ response to emission perturbations is nonlinear due to chemistry as discussed by *Wu et al.* [2009], who found that the perturbation from a 100% $NO_x$ emission reduction yields $O_3$ responses greater than 5 times the 20% $NO_x$ emission reductions. Differencing $O_3$ mixing ratios with sharp gradients in the vicinity of tropopause folds may also introduce noise. Therefore, for each event discussed, we carefully checked for consistent patterns in Asian enhancements to $O_3$, CO, and $NO_y$ in the model, constrained wherever possible by independent observations (e.g., satellite images and ozonesondes).

### 2.5. Emissions

[15] We implement emission inventories to reflect 2010 conditions. All emission inventories described here are regridded to 1° × 1° for C48 and 0.5° × 0.5° for C180. The global emissions from anthropogenic sources and international shipping for the year 2000 (0.5° × 0.5°) were taken from *Lamarque et al.* [2010] as a base inventory. We then replaced anthropogenic emissions in the East Asian domain (13°S–53°N, 70°–150°E) with the 2006 Asian emission inventory (0.5° × 0.5°) from *Q. Zhang et al.* [2009], scaled to 2010 as described below, and the North American (24°–60°N, 135°–40°W) emissions with the U.S. National Emission Inventory (NEI) for 2005 (4 × 4 $km^2$) (ftp://aftp.fsl.noaa.gov/divisions/taq/emissions_data_2005).

[16] For our 2009 and 2010 simulations, North American anthropogenic emissions (including shipping) are held at the 2005 level since changes are expected to be small over this period. We increase the Chinese $NO_x$ emissions from *Q. Zhang et al.* [2009] by 32.6% for 2010 and 27.9% for 2009, based on changes in the 2006–2010 satellite measurements of $NO_2$ columns over central eastern China (30°–40°N, 110°–123°E) from the SCIAMACHY sensor (available on www.tenis.nl, with retrieval technique previously described by *Boersma et al.* [2004]). Our estimate reflects the relatively lower rate of increase of Chinese $NO_x$ emissions during the economic downturn of 2009–2010 [*Lin and McElroy*, 2011] as compared to earlier years [*Q. Zhang et al.*, 2009]. Using $NO_2$ columns directly will tend to overestimate changes in emissions over polluted regions since an increase in $NO_x$ emissions consumes OH and increases the $NO_x$ lifetime, but underestimate changes in emissions over remote regions where an increase in $NO_x$ emissions decreases the $NO_x$ lifetime through feedbacks on $O_3$ and OH [*Lamsal et al.*, 2011]. By considering the influence of $NO_x$ lifetime when deriving emission changes from SCIAMACHY $NO_2$ columns, *Lamsal et al.* [2011] reported a ∼18% increase in Chinese emissions in 2009 relative to 2006. This change is ∼9% lower than our estimate using $NO_2$ columns over polluted central eastern China without adjustments to $NO_x$ lifetime.

[17] We also increase NMVOC emissions in China by 23.2% for 2010 and 17.4% for 2009, relative to 2006, assuming the same annual growth rate as 2001–2006 previously reported by *Q. Zhang et al.* [2009], due to lack of better information. Emissions of $SO_2$, CO, black carbon and organic carbon remain at the 2006 level, based on recent evidence from satellites [*Lu et al.*, 2010; *Lei et al.*, 2011; D. G. Streets, personal communication, 2010].

[18] Daily biomass burning emissions for 2009–2010 are adopted from *Wiedinmyer et al.* [2011] (FINN v1, 1 × 1 $km^2$) and distributed over six ecosystem-dependent altitude regimes between the surface and 6 km, following the recommendations of *Dentener et al.* [2006] as support from recent satellite observations [*Val Martin et al.*, 2010]. Isoprene emissions from vegetation are calculated online based on the Model of Emissions of Gases and Aerosols in Nature

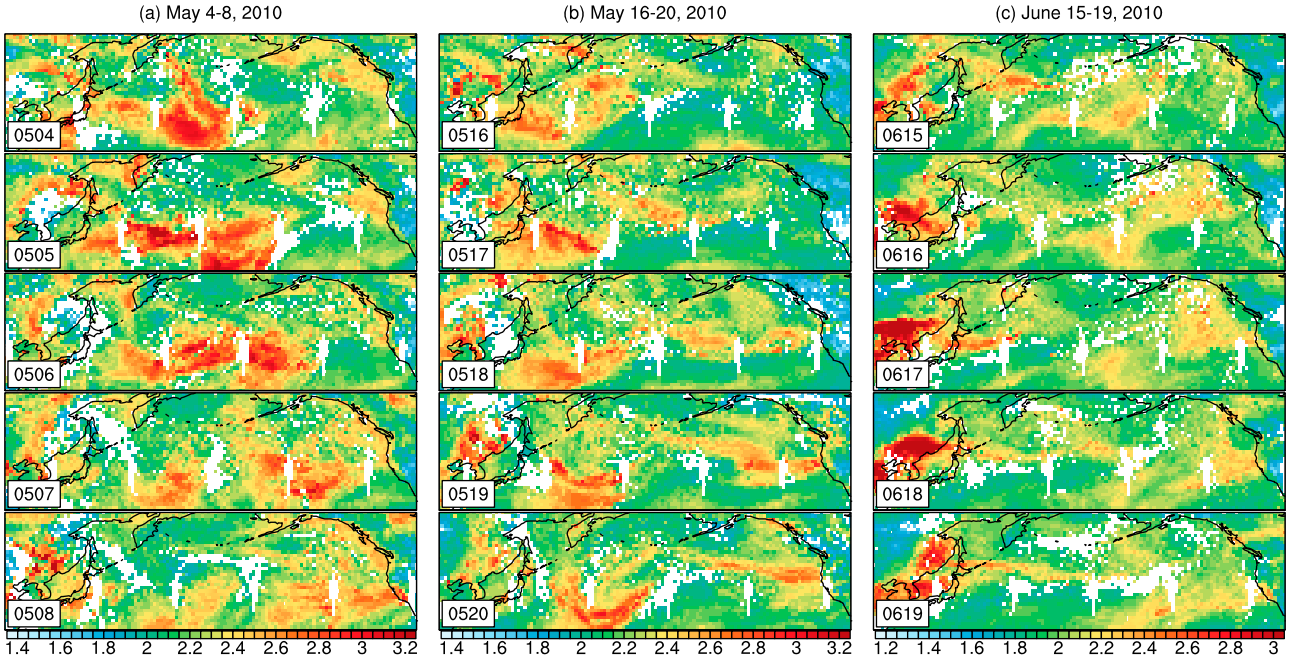


**Figure 1.** (a–c) Major trans-Pacific Asian pollution events in May–June 2010 as seen from AIRS retrievals of CO total columns ($10^{18}$ molecules $cm^{-2}$; level 3 daily 1° × 1° gridded products). Day and nighttime retrievals are averaged, with white areas indicating no retrievals. Data bins are reordered so that neighboring gridded cells of data at the international dateline are no more than a swath of time apart (about 90 min).

(MEGAN) [*Guenther et al.*, 2006], as implemented in *Emmons et al.* [2010] with modifications described by *Rasmussen et al.* [2011]. Other natural emissions–including acetone, ethane, propane, ethylene, propene, methanol, ethanol and monoterpenes from vegetation, CO from vegetation and ocean, volcanic $SO_2$, soil and lightning $NO_x$, dimethyl sulfide (DMS), sea salt and dust–are included as in the standard AM3 simulation [*Donner et al.*, 2011].

## 3. Transport Pathways of Asian Pollution

[19] We identify three major trans-Pacific Asian pollution events from AIRS measurements of daily CO columns for May–June 2010. Figure 1 illustrates the daily progression of these large-scale CO plumes from the East Asian coast to the North American west coast during May 4–8, May 16–20, and June 15–19. These events are typical cases of rapid trans-Pacific warm conveyor belt (WCB) transport [*Cooper et al.*, 2004a]. The June plume (Figure 1c) took a more northerly route to the Gulf of Alaska followed by southeastward advection toward southern California, spending ~1 day longer over the North Pacific Ocean than the two plumes in May. Model CO columns exhibit a similar large-scale structure as the AIRS data, and reveal that these CO plumes are dominated by Asian pollution which was lofted from the continental boundary layer of eastern China approximately 1 week prior to their arrival to the U.S. west coast (figure not shown). Our analysis described below mainly revolves around the three Asian pollution events displayed in Figure 1, the mechanisms governing their transport into western U.S. surface air, and the ability of AM3 to capture these processes.

### 3.1. Cyclone Passages and Merging Air Streams

[20] Prior work has shown that Asian pollution is often intermingled with stratospheric $O_3$ intrusions above the North American west coast [e.g., *Jaeglé et al.*, 2003; *Cooper et al.*, 2004b; *Liang et al.*, 2007; *Ambrose et al.*, 2011]. Indeed, we find that deep tropopause folds occurred one day prior to the arrival of Asian pollution above the California coast on May 18 and June 17, while the May 4–8 pollution event was followed by two consecutive stratospheric intrusions on May 9–11 [*Langford et al.*, 2011; M. Lin et al., Springtime high surface ozone events over the western United States: Quantifying the role of stratospheric intrusions, manuscript in preparation, 2012]. Taking the May 16–20 event as an example, we examine here the dynamic processes leading to the interleaving and mixing of Asian and stratospheric originating air masses and quantify their contributions to $O_3$ entering western North American.

[21] Observed and simulated $O_3$ vertical profiles at two coastal sites from May 17–19 are shown in Figure 2. The GFDL AM3 model (section 2.4) successfully reproduces the layered structure, sharp vertical gradients, and day-to-day variability in the observed $O_3$ profiles, a major improvement upon previous models [*Jaeglé et al.*, 2003; *Liang et al.*, 2007; *Jonson et al.*, 2010].

[22] Figure 3 depicts the evolution of two consecutive midlatitude cyclones sweeping over the Gulf of Alaska and the associated upper level structure during May 17–19. On May 17, AIRS-retrieved total $O_3$ shows a sharp spatial gradient, with a narrow band of elevated $O_3$ columns in excess of 450 DU (Figure 2d) coinciding with an elongated dry air stream in the GFDL AM3 model (Figure 2a), both extending

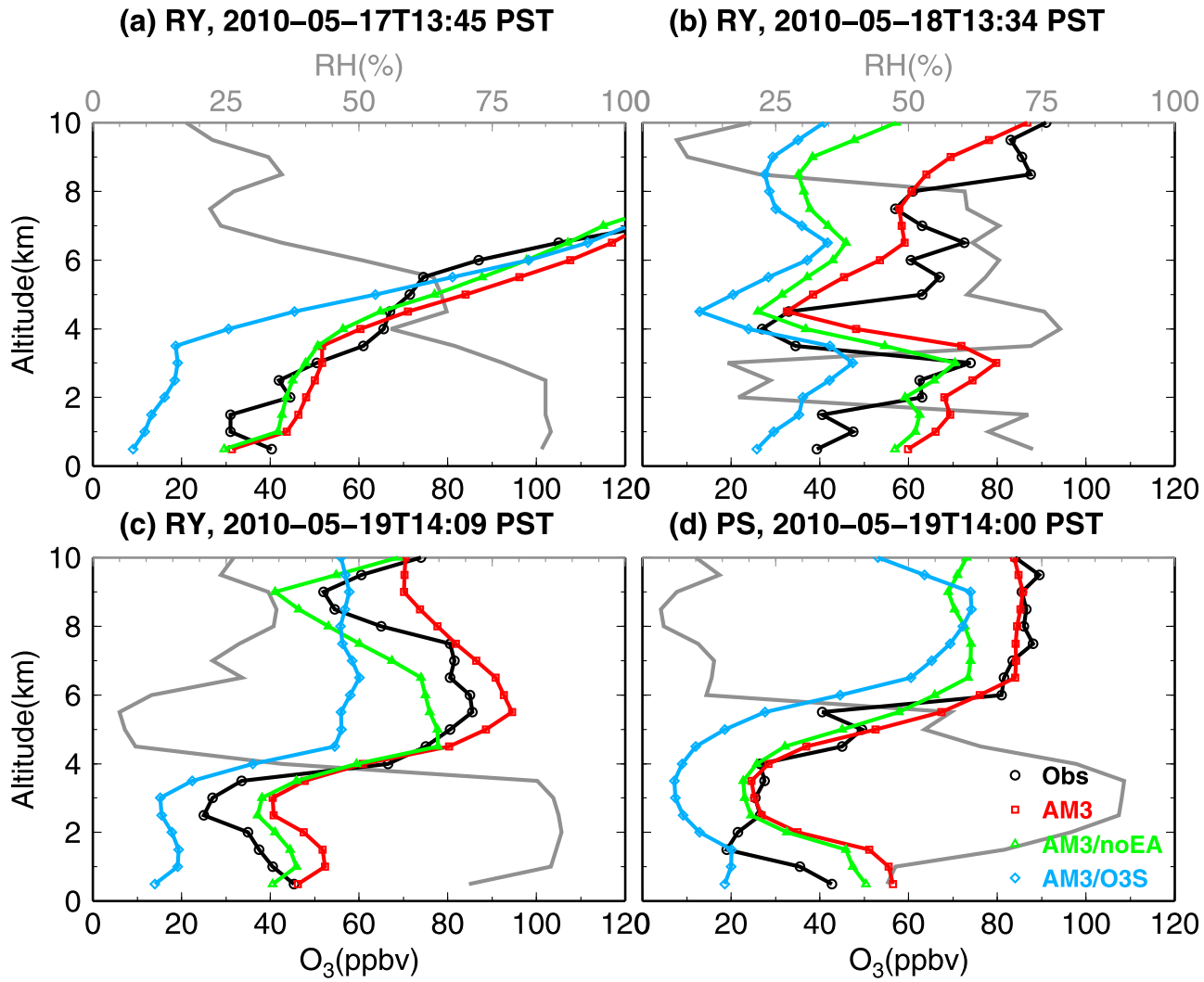


**Figure 2.** (a–d) Observed vertical profiles of relative humidity (gray) and ozone (black) at Point Reyes (RY) and Point Sur (PS) sondes on May 17–19, together with model total ozone (red), stratospheric ozone tracer (blue), and model ozone from a sensitivity simulation with Asian anthropogenic emissions shut off (green). Model results have been interpolated to the sonde pressure and averaged over 0.5-km altitude bins.

to the California coast. This typical feature of a stratospheric intrusion [*Wimmers et al.*, 2003; *Felker et al.*, 2011] is also represented in the GFS FNL analysis by the potential vorticity (PV) contours on the 300 hPa surface. The ozonesonde launched at Point Reyes, located immediately to the right of the tropopause fold off the California coast, recorded high $O_3$ mixing ratios in excess of 100 ppbv penetrating down as low as 6 km a.s.l. (Figure 2a), coincident with low humidity, a marker for air of stratospheric origin.

[23] Between May 17 and 18, this dry air stream of stratospheric origin sheared into three components in a similar manner previously described by *Cooper et al.* [2004b]. Depicted in the AIRS retrievals of total column $O_3$ and model 300–400 hPa humidity on May 18 (Figures 3b and 3e), the first component travels across the western U.S. with the upper level flow, while the second component representing the bulk of the dry air stream moves northward. A three dimensional view of AM3 stratospheric $O_3$ tracer reveals that the third component had descended into the lower troposphere by 21:00 UTC, May 18, leading to the formation of a distinct $O_3$ layer just 2 km above the California coast (Figure 4a). Four ozonesondes launched along the California coast on May 18 confirm the existence of this dry layer of enhanced $O_3$ (Figure S3, middle panels). Transported stratospheric remnants contribute 40–80 ppbv to the simulated 60–100 ppbv range of total $O_3$ mixing ratios in this approximately 2 km thick layer of enhanced $O_3$, with collocated CO enhancements (Figure 4b). AIRS observations of CO columns indicate transport of an Asian pollution plume into the eastern North Pacific on May 18 by the WCB of the next midlatitude cyclone entering this region (Figure 1a). We find in the model that the bulk of Asian polluted air masses were located in the upper troposphere (6–10 km) (Figure 4b), immediately adjacent to stratospheric air on the left (Figure 4a). Asian anthropogenic emissions contribute 20–30% of total $O_3$ mixing ratios in the upper troposphere when the air was sampled by the Point Reyes ozonesonde on May 18 (Figure 2b). Similar to the findings of *Stohl and Trickl* [1999], these processes reveal two interleaving $O_3$ layers with dominating stratospheric and

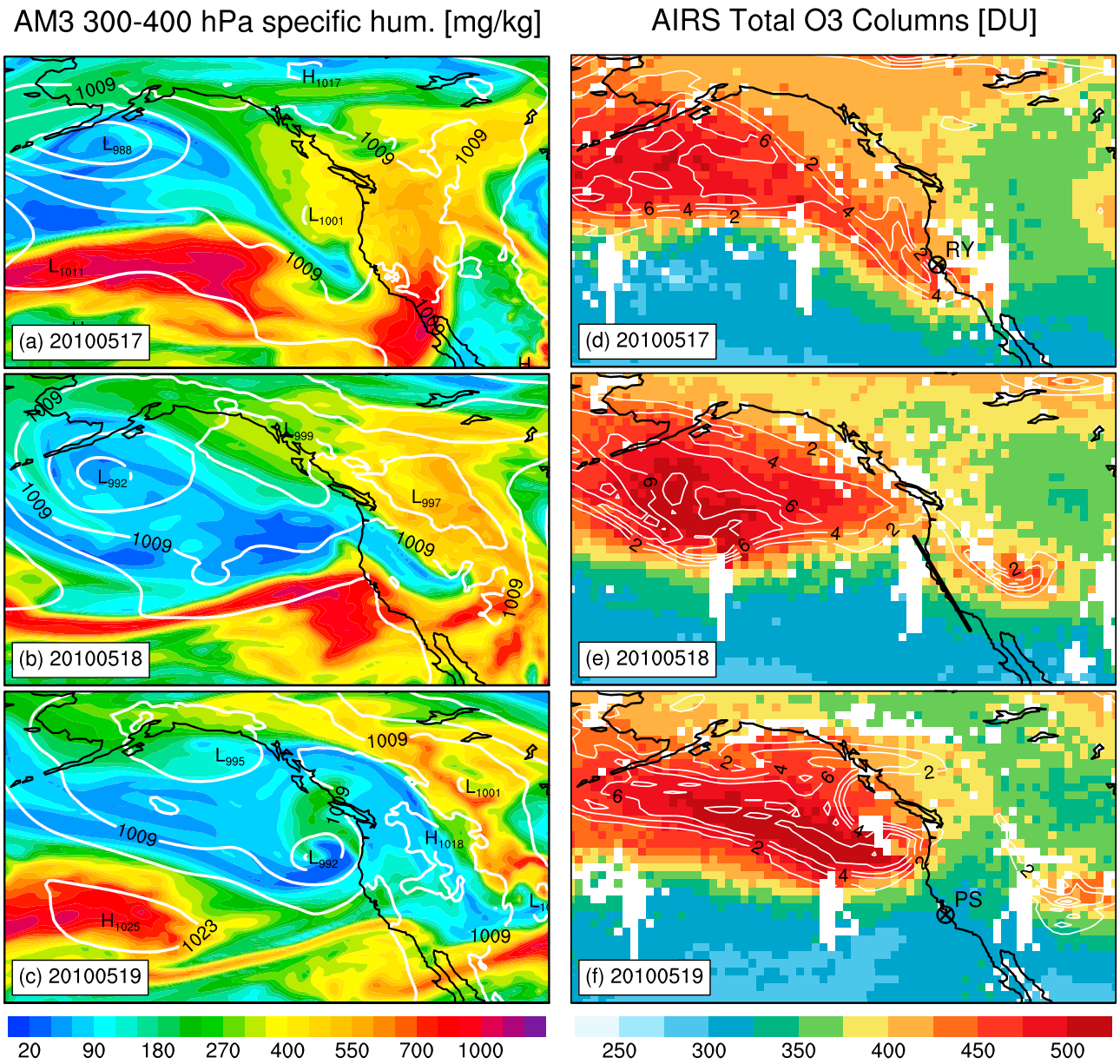


**Figure 3.** Evolution of two midlatitude cyclones and associated flow structures over the Pacific North America on May 17–19, 2010. Shown are (a–c) AM3 6-h mean sea level pressure (contours, hPa) with 300–400 hPa layer average specific humidity (shading, mg/kg) at 21:00 UTC and (d–f) AIRS retrievals of daily mean total column amounts of ozone (shading, DU) with 300 hPa potential vorticity (contours, PVU) computed from GFS Final analysis at 18:00 UTC. Only PV values greater than 2 PVU are contoured and signify air of essentially stratospheric origin. The thick black line along the California coast in Figure 3e indicates the location of vertical cross-section shown in Figure 4.

Asian influence in the lower and upper troposphere, respectively.

[24] By 21:00 UTC, May 19, the first cyclone decayed and a newly formed cyclone was located off the coast of Washington (Figure 3c). A portion of stratospheric air that had rolled back from the deep intrusion on May 17 was now entrained into the newly formed tropopause fold of the second cyclone (Figure 3f). A distinct high-$O_3$ layer with lower humidity between 4 and 8 km a.s.l. was observed by the Point Reyes and Point Sur ozonesondes and successfully captured by the model (Figures 2c and 2d). In the ~60–95 ppbv of simulated total $O_3$ in this layer, remnants of stratospheric intrusions and Asian anthropogenic emissions contribute ~40–55 ppbv and 10–25 ppbv, respectively, suggesting the intermingling of polluted and stratospheric air.

[25] Between May 19 and 20, stratospheric and Asian polluted air masses became further intermingled and descended into the mid- and lower troposphere above southern California (Figure S2). These air masses reached the western U.S. surface on May 20–21, contributing to elevated surface $O_3$ episodes in the national parks (section 5.2).

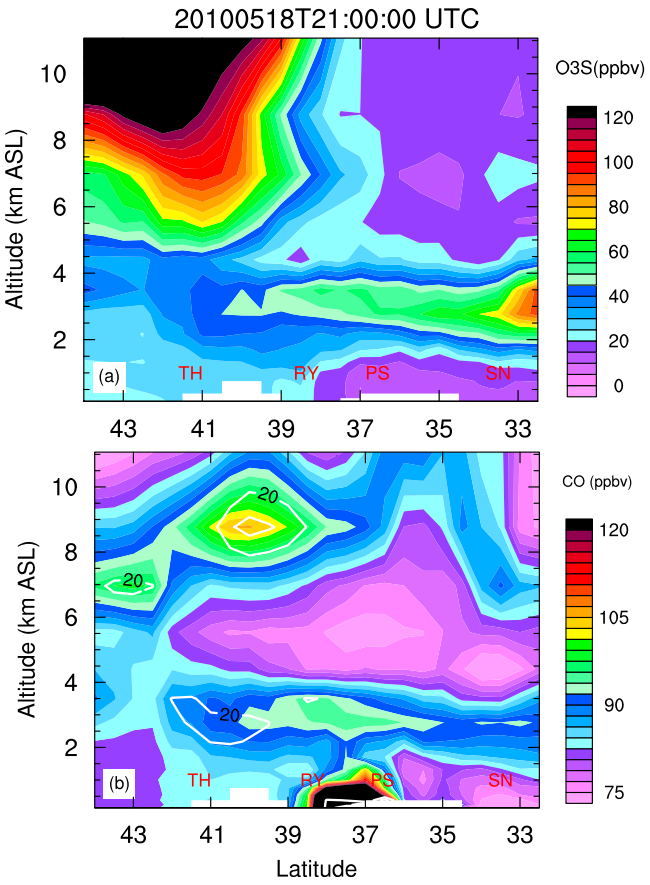


**Figure 4.** Vertical cross-section along California coast (thick black line in Figure 3e), Showing (a) simulated stratospheric ozone tracer (shading, section 2.3) and (b) total CO (shading) with Asian CO (contoured every 5 ppb starting at 20 ppb) as determined by the difference between the standard simulation and a sensitivity simulation with Asian anthropogenic emissions shut off. Letters in red denote locations of ozonesondes (Figure S1).

[26] Other stratospheric intrusions identified during the CalNex campaign were also mixed, to varying degrees, with Asian pollution, suggesting that the dispersion of $O_3$-rich stratospheric air into polluted air masses is a common feature in the vicinity of active storm tracks in the North Pacific as well as in the Atlantic [e.g., *Stohl and Trickl*, 1999; *Parrish et al.*, 2000; *Esler et al.*, 2003]. Our analysis further supports prior publications suggesting that a positive $O_3$-CO correlation does not necessarily indicate anthropogenic influence on $O_3$ enhancements in the continental outflow (such as Asian Pacific Rim) or inflow regions (such as North American west coast) [*Cooper et al.*, 2004b; *Voulgarakis et al.*, 2011]. Thus the $O_3$-CO correlations derived from collocated in situ or satellite measurements (such as TES) reported in earlier studies [e.g., *Zhang et al.*, 2006, 2008; *Voulgarakis et al.*, 2011; *Pfister et al.*, 2011] should be interpreted with caution.

### 3.2. Isentropic Transport Mechanisms

[27] We explore here the transport of Asian pollution into western U.S. surface air and its impacts on the regional variability in surface $O_3$, focusing on the Asian pollution event in June (Figure 1c). Figure 5 shows observed and simulated $O_3$ profiles at Trinidad Head and Point Reyes on June 17–19, illustrating a layered structure of $O_3$ with stratospheric and Asian origin, similar to those discussed in section 3.1. The large Asian influence on $O_3$ mixing ratios (up to 30 ppbv) mainly occurred between ~3 and 9 km above the California coast during June 17–19. Less stratospheric $O_3$ was entrained into the polluted WCB during this event than during May 19–20. This Asian pollution plume was transported into the California coast by the WCB of a midlatitude cyclone, which intensified and moved into the Gulf of Alaska during June 19–21 (Figure S4). A southeastward shift of the Pacific anticyclone and a weak surface low extending northward from Mexico produced onshore flow, containing Asian pollution, across central and southern California. These conditions led to a strong latitudinal variation of Asian CO which descends along isentropic surfaces (S4), a typical feature of Asian plumes entering the western U.S. [*Brown-Steiner and Hess*, 2011]. By 21:00 UTC, June 20, the plume has progressed to southern California, with the vertical distribution of Asian $O_3$ up to 10–30 ppbv exhibiting a continuous band sloping from 5 to 8 km a.s.l. all the way to the surface of the Sierra Nevada and southern California (Figure 5d).

[28] The subsiding Asian pollution along isentropic surfaces episodically enhances surface $O_3$ levels above the surrounding "background" over the intermountain regions. Figure 6 shows that the regions experiencing high Asian influence in excess of 8–15 ppbv are where the observed and simulated total $O_3$ pattern is enhanced. The model estimates Asian enhancements of 8–15 ppbv in locations where observed MDA8 exceeds 60 ppb on June 20–22 over the intermountain west, and of 5–8 ppbv where observed MDA8 exceeds 75 ppb over parts of southern California on June 22. While these estimates are likely an upper limit for current conditions (see section 2.4), they nevertheless indicates the potential for Asian emissions to contribute to high-$O_3$ episodes over the high-altitude western USA.

[29] Asian influence appears to be minimal where $O_3$ exceeds 75 ppbv in the Central Valley of California on June 21–22 (Figure 6), indicating that this $O_3$ pollution mostly reflects photochemical production from local emissions and suppressed ventilation under the influence of a surface anticyclone. *Langford et al.* [2010] suggested that $O_3$ produced in the LA Basin can be lifted by topographic venting, followed by westerly transport to Utah and western Colorado. An additional sensitivity simulation with North American anthropogenic emissions switched off in the model suggests that North American influence is relatively smaller over the intermountain regions where the model suggests Asian enhancements contribute to enhancing total surface $O_3$ than at the local pollution hot spots around each city (Figure S6). We note that the ~50 × 50 km$^2$ horizontal resolution of AM3 may be insufficient to capture the meso-scale mountain-valley flows described by *Langford et al.* [2010].

[30] Another notable feature in Figure 6 is the modeled $O_3$ minimum above the ocean that parallels the coast and varies strongly with distance from shore. This $O_3$ minimum largely reflects the influence of the low-level jet along the California coast which is typically at a maximum in summer [*Burk and Thompson*, 1996; *Parish*, 2000]. The lower observed $O_3$ at the AQS sites near the coast supports the existence of this

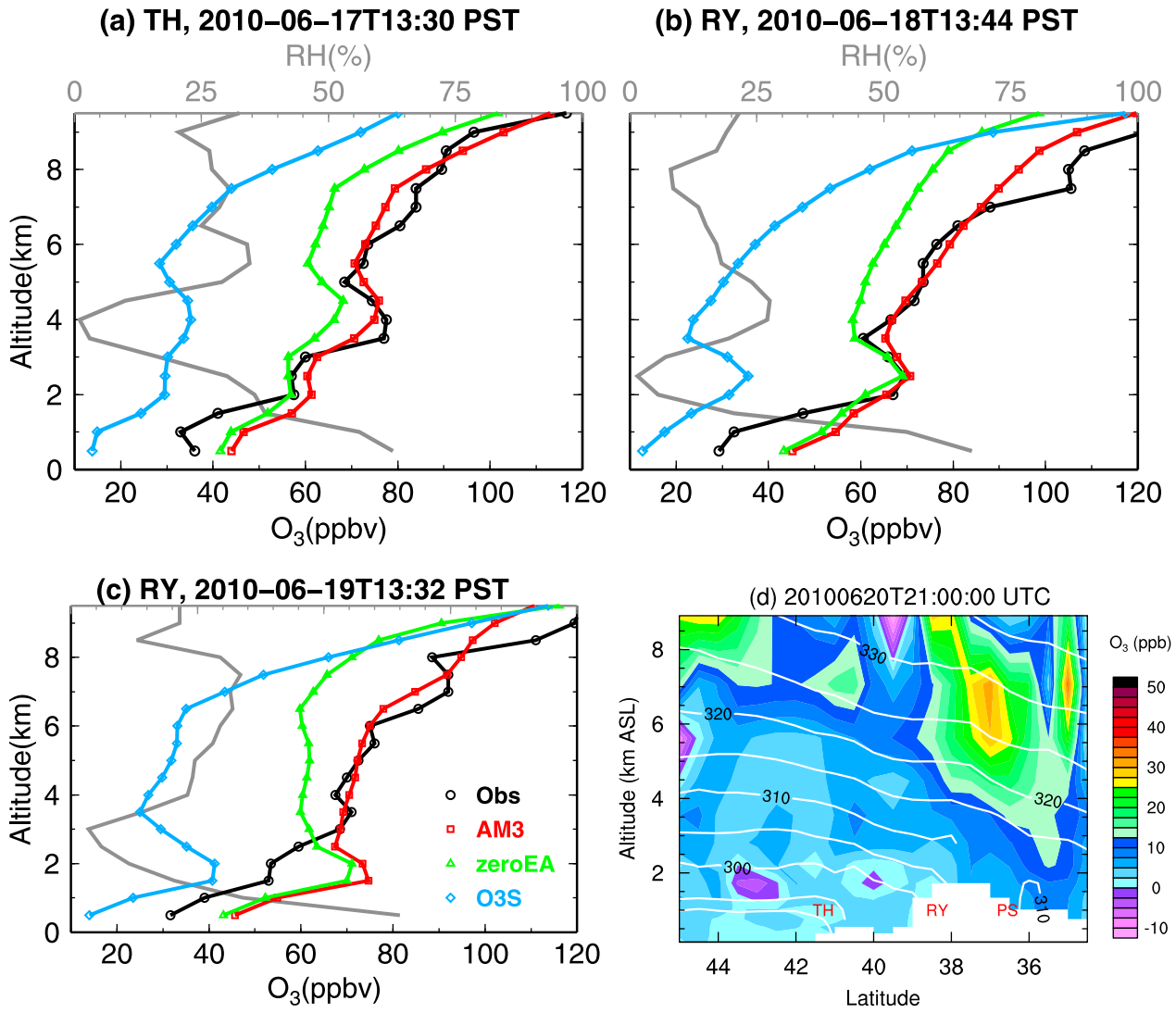


**Figure 5.** (a–c) As in Figure 2, but for the June 17–19 event at Trinidad Head (TH) and Point Reyes (RY). (d) Subsidence of Asian ozone (shading) along isentropic surfaces (contours, K) above the California coast on June 20, 2010 (also see Figure S4).

transport pattern. Asian enhancements to $O_3$ in the coastal marine boundary layer do not exhibit strong episodic variations, consistent with prior publications regarding background influence at the Trinidad Head surface site [*Goldstein et al.*, 2004; *L. Zhang et al.*, 2009; *Parrish et al.*, 2010; *Cooper et al.*, 2011]. Our results further reveal that the majority of the Asian pollution plumes arriving to the U.S. west coast are located in the free troposphere where a portion of the pollution descends isentropically behind cold fronts, which is directly intercepted by the elevated terrain and eventually becomes entrained into the daytime boundary layer over land. This transport mechanism is the key driver for the stronger signal of episodic Asian pollution in surface air over the U.S. intermountain regions than over the North Pacific Ocean.

### 3.3. Dispersion of Asian Pollutants Into Southwestern U.S. Surface Air

[31] We discuss in this section the potential impacts of Asian pollution in a densely populated region like the LA Basin, where Asian pollution can mix with high levels of locally produced $O_3$ pollution. The NOAA WP-3D intercepted a pollution layer approximately 2 km above the LA Basin on May 8, with 3–8 $\mu g/m^3$ sulfate aerosol, < 1 $\mu g/m^3$ organic mass, 150–175 ppbv CO, and 80–90 ppbv $O_3$ (Figure 7). This pollution layer was encountered three times (denoted as red arrows in Figure 7c) by the aircraft, and shows distinct sulfate enhancements, in contrast to the boundary layer pollution with dominant signatures of primary emissions (such as organic matter and CO). The observed high sulfate concentration is unlikely to be from oxidation of $SO_2$ emissions from diesel ships off California's coast. GOES 1 km visible images for this day show that the weather was calm and the skies completely cloud free above southern California and the nearby offshore regions, indicating no vertical transport of moist marine boundary layer air up to 2 km a.s.l. Under these types of conditions aircraft in situ observations of ship plumes off the California coast show that the plumes remain within the very stable marine boundary and are less than 200 m above the surface [*Chen*

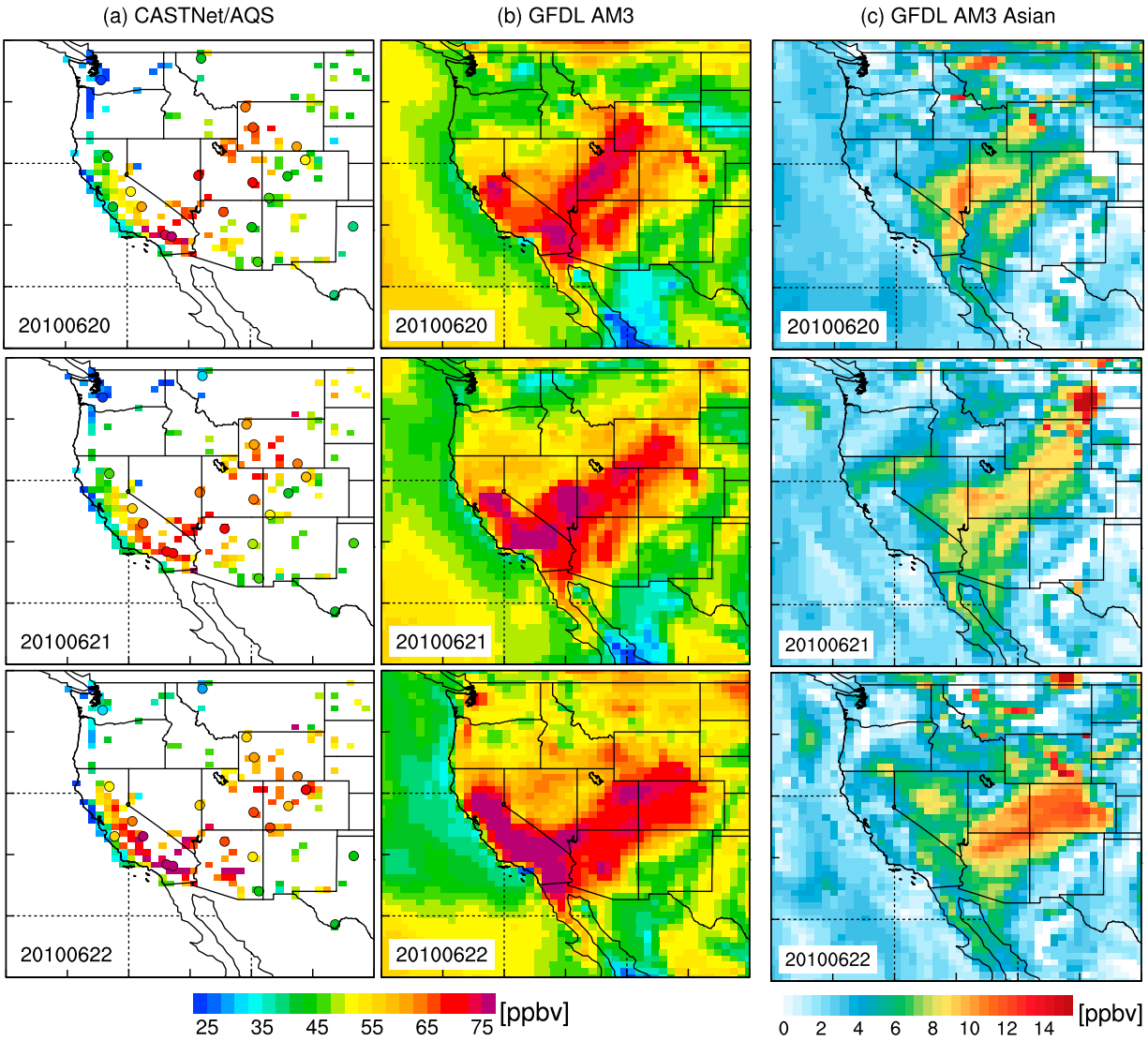


**Figure 6.** Spatial patterns of daily maximum 8-h average ozone in western U.S. surface air on June 20–22, 2010, showing (a) CASTNet (circles) and AQS (squares) observations, (b) results from the surface layer in the GFDL AM3 model, and (c) the enhancements due to Asian anthropogenic emissions, calculated using the same 8-h interval identified for the MDA8 in the base simulation.

*et al.*, 2005]. The presence of an aerosol layer dominated by sulfate is a distinguishing feature of Asian pollution layers that have been transported to the eastern North Pacific [*Brock et al.*, 2004; *Peltier et al.*, 2008; *Dunlea et al.*, 2009]. When a polluted air mass rises out of the Asian boundary layer, the existing aerosol is washed out if precipitation occurs during lifting, while the less-soluble gas phase compounds such as $SO_2$ are not entirely removed. $SO_2$ that "escaped" wet removal during lifting is converted into sulfate during subsequent trans-Pacific transport in the free troposphere, enhancing the sulfate-to-organic aerosol ratio in eastern North Pacific air masses influenced by Asian pollution.

[32] Indeed, AIRS CO retrievals confirm the occurrence of large-scale trans-Pacific transport of Asian pollution during May 4–8 (Figure 1a). The plume arrived at the coast of California on May 8, evident both in AIRS CO and in the AM3 model Asian enhancements to tropospheric column $O_3$ (Figure 7a). A vertical cross-section of model Asian $O_3$ in Figure 7b depicts a plume-like feature of Asian $O_3$ enhancements in excess of 10–25 ppbv sloping from 3 to 6 km above northern California to 2–3 km above the LA Basin where the air masses were sampled by the WP-3D. Other WP-3D flights during CalNex also intercepted sulfate-dominated aerosol layers above California, to varying degrees, on May 7, May 24, and June 20. The model indicates Asian enhancements to $O_3$ mixing ratios but fails to reproduce the magnitude of sulfate concentrations, likely due to excessive wash out during trans-Pacific transport consistent with an overestimate in precipitation [*Donner et al.*, 2011].

[33] Our analysis suggests that the signature of Asian pollution enhancements in the lower troposphere of the densely populated LA Basin is sufficiently strong to be observed, such as through analysis of chemical composition demonstrated here. Daytime mixed layers in this region

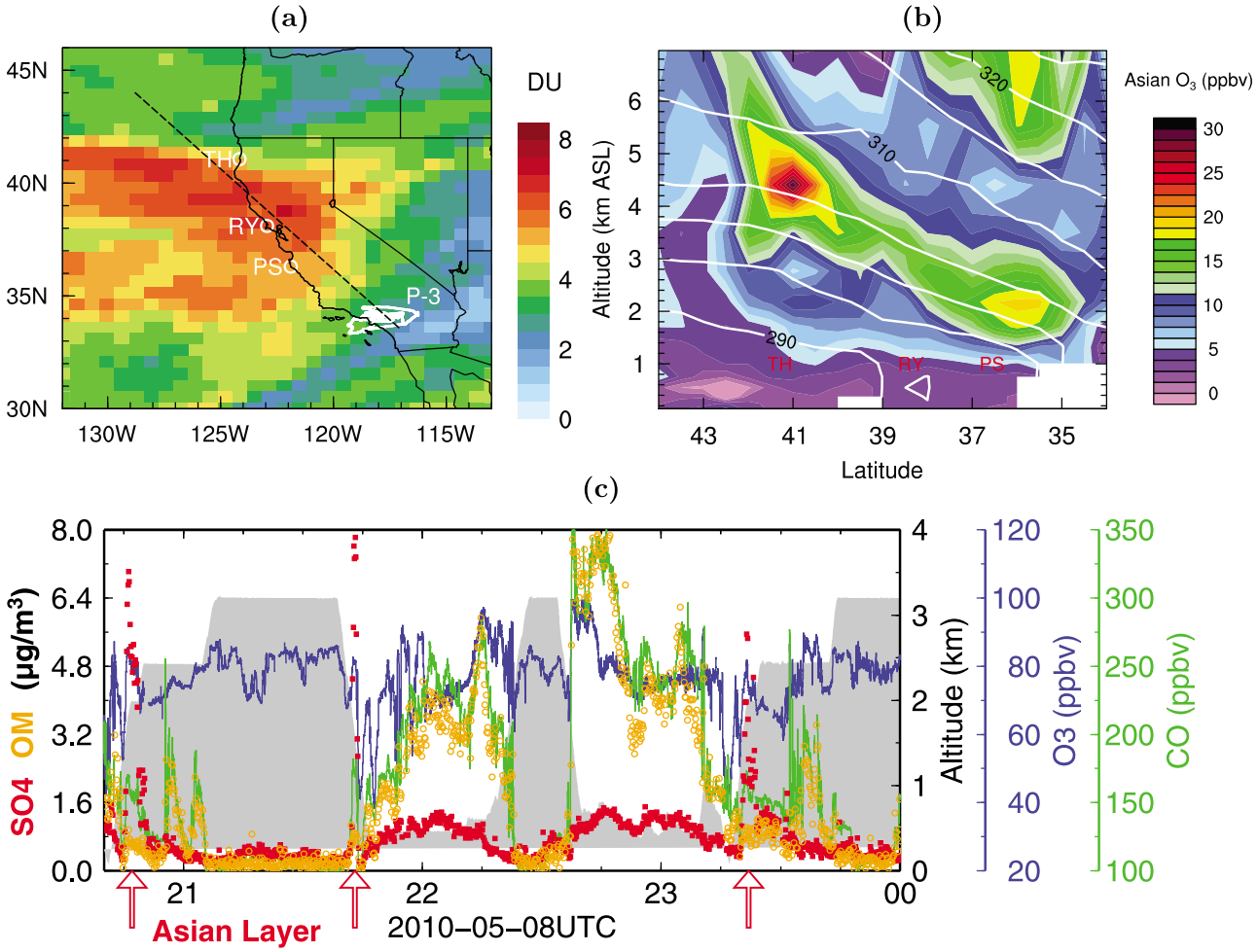


**Figure 7.** Transport of Asian pollutants to the lower troposphere of southern California on May 8, 2010. (a) Model Asian enhancements to the tropospheric column $O_3$ in dobson unit. The dashed black line denotes the location of the ozone vertical cross-section shown in Figure 7b. The white line indicates the NOAA WP-3D flight path. (b) Model vertical distribution of Asian ozone (shading) with isentropic surfaces (contours, K) along the California coast. (c) Observed distributions of CO (green), O3 (blue), sulfate (red) and organic aerosols (orange) along the WP-3D flight path, with altitude shown as gray shading.

range from 1 to 4 km a.s.l. [*Langford et al.*, 2010; *Cooper et al.*, 2011; *Neuman et al.*, 2012; D. Seidel et al., Climatological variations in planetary boundary layer mixing heights over the Continental United States and Europe, submitted to *Journal of Geophysical Research*, 2011]. Asian pollution ~2 km aloft is thus available to be entrained into the boundary layer and contributes to the local pollution burden. It should be noted that strong dilution may occur when Asian polluted air masses are dispersed into the boundary layer. For example, Figure 8 shows that much of Nevada experiences a pronounced maximum of Asian enhancements (10–15 ppbv) to surface $O_3$ on May 8, primarily reflecting the free tropospheric signal intersected by the elevated terrain. By May 9, Asian influence covers a larger spatial extent (including southern California), but the magnitude is weakened by a factor of two. Observed $O_3$ at the CASTNet and AQS ground stations exhibits a similar day-to-day variability in the spatial pattern as model surface $O_3$. Despite dilution, Asian emissions contribute at least 50% of the surface $O_3$ increases from May 8 to May 9 over Arizona and western Colorado.

## 4. Model Evaluation

### 4.1. Variability and Bias in $O_3$ Flowing Into the Western U.S.

[34] Generalizing from the process-oriented analysis in sections 3.1–3.3, we conclude that the GFDL AM3 model captures much of the observed dynamic variability in $O_3$ flowing into the western U.S. resulting from complex air stream interactions. A systematic evaluation of model $O_3$ profiles at seven ozonesonde sites during CalNex shows that AM3 captures the latitudinal variation of surface to near tropopause $O_3$ along the California coast, with correlation coefficients for day-to-day variability ranging from 0.50 to 0.96 (Lin et al., manuscript in preparation, 2011). For most cases, AM3 at C48 horizontal resolution (~163–231 km) also captures the general features of the observed $O_3$ profiles (Figures S3 and S5). The model bias in the upper

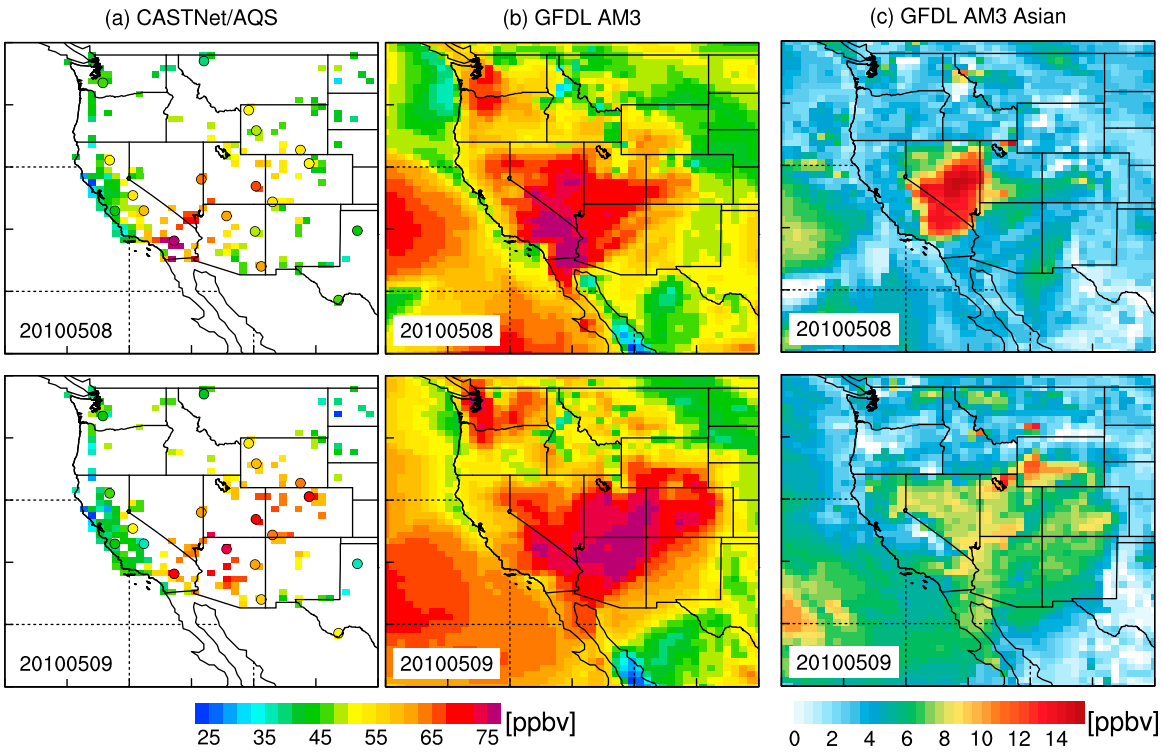


**Figure 8.** As in Figure 6, but for May 8–9, 2010.

troposphere tends to increase when the ozonesondes are primarily influenced by stratospheric air, likely due to limitations to resolve adequately (at both C48 and C180) the filamentary structure of tropopause folds and the associated sharp vertical and horizontal gradients in $O_3$ mixing ratios.

### 4.2. Variability and Bias in Ground-Level $O_3$

[35] Table 1 summarizes the model mean bias in MDA8 $O_3$ and correlation coefficients at 18 CASTNet sites over the western USA during May–June 2010. Despite the large bias (up to 10–25 ppbv) at the coastal sites (e.g., at MOR, PIN, LAV), the model reproduces much of the day-to-day variability in surface $O_3$ with correlation coefficients ranging from 0.4 to 0.8 and standard deviations within 15% of those observed for most CASTNet sites. Comparison with AQS observations (Figure S7) further shows that the model captures the regional variability of mean observed surface $O_3$ over the western U.S., including a minimum in the coastal areas and a maximum in the southern California and intermountain regions. The surface $O_3$ bias is typically smaller at the high-elevation sites over the intermountain regions, suggesting that downward transport from the free

**Table 1.** May–June 2010 Mean Statistics for Observed and Model MDA8 $O_3$ in Surface Air at the CASTNet Ground Stations in the Western USA

| State | Site ID | Site Name | Elevation (m) | Observed[a] (ppbv) | Model[a] (ppbv) | *R* |
|---|---|---|---|---|---|---|
| AZ | GRC474 | Grand Canyon NP | 2073 | 59 ± 7 | 64 ± 8 | 0.56 |
| AZ | PET427 | Petrified Forest | 1723 | 56 ± 7 | 62 ± 9 | 0.46 |
| AZ | CHA467 | Chiricahua NM | 1570 | 57 ± 7 | 60 ± 11 | 0.67 |
| CA | PIN414 | Pinnacles NM | 335 | 46 ± 7 | 62 ± 10 | 0.83 |
| CA | YOS404 | Yosemite NP | 1605 | 53 ± 10 | 61 ± 10 | 0.73 |
| CA | LAV410 | Lassen Volcanic NP | 1756 | 48 ± 8 | 60 ± 8 | 0.80 |
| CA | JOT403 | Joshua Tree NP | 1244 | 74 ± 12 | 72 ± 8 | 0.42 |
| CA | SEK430 | Sequoia NP - Ash Mountain | 457 | 59 ± 13 | 70 ± 10 | 0.80 |
| CO | MEV405 | Mesa Verde NP | 2165 | 55 ± 8 | 64 ± 8 | 0.60 |
| CO | ROM406 | Rocky Mtn NP | 2743 | 59 ± 10 | 61 ± 10 | 0.72 |
| CO | ROM206 | Rocky Mtn NP Collocated | 2743 | 55 ± 11 | 61 ± 11 | 0.75 |
| NV | GRB411 | Great Basin NP | 2060 | 54 ± 9 | 61 ± 10 | 0.71 |
| TX | PAL190 | Palo Duro | 1050 | 49 ± 7 | 54 ± 7 | 0.46 |
| TX | BBE401 | Big Bend NP | 1052 | 49 ± 8 | 50 ± 7 | 0.54 |
| UT | CAN407 | Canyonlands NP | 1809 | 58 ± 7 | 65 ± 9 | 0.57 |
| WA | MOR409 | Mount Rainier NP | 415 | 29 ± 8 | 55 ± 5 | 0.71 |
| WY | PND165 | Pinedale | 2388 | 53 ± 8 | 58 ± 8 | 0.69 |
| WY | CNT169 | Centennial | 3178 | 56 ± 8 | 58 ± 8 | 0.55 |

[a]Mean ± standard deviation.

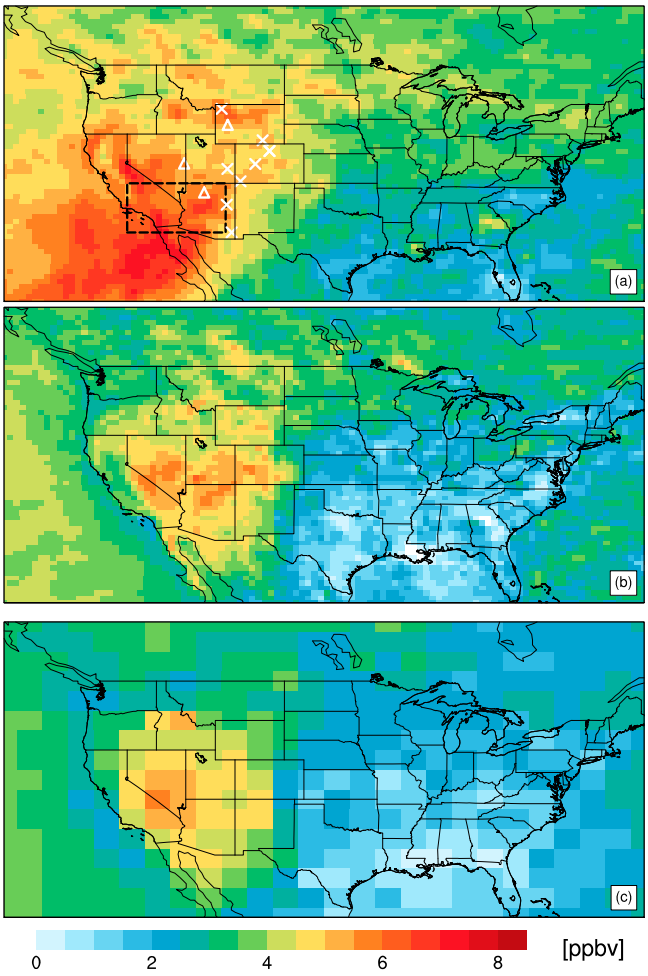


**Figure 9.** Asian pollution enhancements to (a) mean ozone mixing ratios at ~800 hPa and (b) daily maximum 8-h ozone in surface air for May–June 2010, estimated with ~50 km AM3. (c) Same as Figure 9b, but for ~200 km AM3. The dashed rectangle in Figure 9a indicates the surface region analyzed in Figure 10. The symbols denote locations of 12 CASTNet high-elevation sites shown in Figure S8b.

troposphere is not likely to be the primary cause of the surface $O_3$ bias. Supporting this conclusion, we find that the model bias in surface $O_3$ at both the low-elevation AQS sites and high-elevation CASTNet sites does not have a direct relationship with the Asian enhancement (Figure S8).

### 4.3. Ozone Production Efficiency

[36] Next we evaluate the $O_3$ production efficiency (OPE), $O_x$ versus $NO_z$ derived from collocated measurements of $O_3$, $NO_x$, and $NO_y$ aboard the WP-3D aircraft during CalNex, over the LA Basin and the Central Valley, respectively (Figure 9). The observations suggest a slightly smaller OPE in the LA Basin than Central Valley. The model captures this urban versus rural difference in OPE [*Trainer et al.*, 1993; *Kleinman et al.*, 1994], with the slope of $O_x$ versus $NO_z$ linear least squares correlation within ~10% of those observed for both regions. The intercept of the correlation can be interpreted as a background $O_3$ level [*Kleinman et al.*, 1994]. We find that the intercept of $O_x$ versus $NO_z$ over the LA Basin in the model is close to that in the observations (Figure S9a). For the Central Valley (Figure S9b), however, the intercept is ~10 ppbv higher in the model, suggesting a possible problem in the boundary layer "background" $O_3$ level over this region. Figure S10 confirms that the bias gets worse in the low tail of the cumulative probability distribution of $O_3$ in the Central Valley.

[37] We conclude that the model has systematic positive biases in the northern California and coastal regions. While the source of this problem is unclear, it may reflect some combined influence from model limitation in resolving coastal gradients and sharp topography, an underestimate in coastal marine boundary layer cloudiness [*Donner et al.*, 2011] which affects oxidant production and loss, local $NO_x$ emissions or lifetime, and planetary boundary layer mixing heights (MH). A systematic evaluation of continental U.S. boundary layer MH in GFDL AM3 indicates that the model reproduces general features of observed spatial, seasonal, and diurnal MH variability but has difficulty simulating shallow, stable boundary layers at night (Seidel et al., manuscript in preparation, 2011).

## 5. Impacts of Asian Pollution on U.S. Surface Ozone Air Quality

### 5.1. Mean Distributions

[38] Figure 9a shows the mean Asian anthropogenic enhancement to U.S. $O_3$ mixing ratios at ~800 hPa averaged over May–June 2010; a pronounced maximum occurred over the southwestern U.S. Enhanced Asian pollution in the lower troposphere toward the south reflects the combined influence from isentropic subsidence (section 3) and production of $O_3$ from $NO_x$ released from the thermal decomposition of Asian PAN when the air warms as it descends (Figure S11). Earlier studies suggest that Asian pollution reaching the eastern North Pacific Ocean typically splits into northern and southern branches with $O_3$ production due to PAN decomposition occurring in the southern branch [e.g., *Moxim et al.*, 1996; *Heald et al.*, 2003; *Hudman et al.*, 2004; *Zhang et al.*, 2008; *Fischer et al.*, 2010, 2011]. We find that this mechanism extends into the western U.S. during spring 2010 and contributes to the total Asian enhancement to surface $O_3$.

[39] The spatial pattern of Asian enhancements at ~800 hPa is in general agreement with forward trajectory analysis of surface destinations of baseline air masses by *Cooper et al.* [2011] for the same study period. Our results suggest that the latitudinal variation of the Asian enhancement contributes to $O_3$ gradients along the California coast as measured by ozonesondes [*Cooper et al.*, 2011]. Compared with the springtime climatological pattern of Asian $O_3$ tracer of *Brown-Steiner and Hess* [2011], our May–June 2010 estimates of Asian influence in southwestern U.S. surface air are relatively larger, likely reflecting the southeastward extension of the Pacific storm tracks following an El Niño (section 2.1).

[40] Figure 9b shows the mean Asian influence on MDA8 $O_3$ in the model surface layer for May–June 2010. Trans-Pacific transport of Asian pollution has the greatest impacts on surface $O_3$ in the high-elevation regions over the western

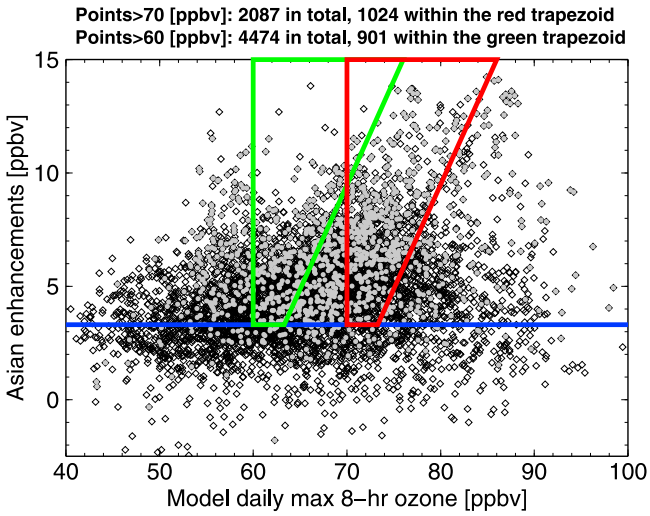


**Figure 10.** Asian enhancements to daily maximum 8-h average ozone in surface air, as estimated with the GFDL AM3 model, plotted as a function of total ozone abundances for all land grids within the rectangle indicated in Figure 9a. The blue line represents the 25th percentile value of Asian enhancements. Points falling within the green and red trapezoids denote values in excess of 60 and 70 ppbv, respectively, that would not have occurred in the absence of Asian emissions in the model. The case study periods in section 3 are identified as gray points.

U.S., consistent with prior studies [e.g., *TFHTAP*, 2011; *Brown-Steiner and Hess*, 2011; *Zhang et al.*, 2011], where the elevated terrain has a higher probability of intersecting subsiding air masses behind cold fronts than lower elevation regions such as the Central Valley of California and the eastern U.S. (section 3). The minimum Asian $O_3$ enhancement in surface air occurs in the Southeast U.S. where the average transport in the lower troposphere advects air masses from the Gulf of Mexico, limiting the influence of westerly transport, similar to summertime transport conditions discussed by *Fiore et al.* [2002]. The AM3 simulation at C48 horizontal resolution (Figure 9c) produces a consistent large-scale view of Asian influence in surface air over U.S., but the high-resolution model spatially refines the estimates and produces a 1–2 ppbv higher impact at the surface in Utah, Arizona and western Colorado. *Zhang et al.* [2011] also found a greater background impact in a nested version of the GEOS-Chem model than the coarser output from the 2° × 2.5° version.

### 5.2. Contribution to Air Quality Exceedances

[41] We next examine in Figure 10, the $O_3$ enhancement from Asian anthropogenic emissions for the entire distribution of springtime MDA8 $O_3$ concentrations in the model surface layer over the southwestern U.S. (box in Figure 9a). Asian emissions can contribute up to 8–15 ppbv when springtime total $O_3$ concentrations exceed 70 ppbv over southern California and Arizona, consistent with case study results in section 3 (gray points in Figure 10). This finding is in contrast to an earlier study indicating that foreign influence typically declines below 8 ppbv in the 70–90 ppbv range of U.S. summertime total $O_3$ concentrations in surface air [*Fiore et al.*, 2002]. While local emissions likely play a dominant role in producing the high-$O_3$ events in surface air over this region, here we calculate the number of $O_3$ events in excess of 60, 70 and 75 ppbv thresholds that would not have occurred in the model in the absence of Asian pollution enhancements. These points are denoted by the green and red trapezoids in Figure 10 for 60 and 70 ppbv thresholds, respectively. We include only points where the Asian enhancement is above the 25th percentile to filter out model noise. Dividing the number of points falling within these trapezoids by the total number of points exceeding the threshold value, we estimate that 20% of MDA8 $O_3$ exceedances of 60 ppbv in the model would not have occurred over southern California and Arizona in the absence of Asian anthropogenic emissions. For a 70 ppbv threshold, this statistic increases to 49% since both the mean and extreme events of Asian enhancements increase in the 70–80 ppbv range of total $O_3$ and the number of exceedances for the 70 ppbv threshold decreases as compared with the 60 ppbv threshold. For a 75 ppbv threshold–the current NAAQS for $O_3$–that statistic is 53%.

[42] We further examine any influence of model biases on the relationship between Asian enhancements and total $O_3$ abundances, and thereby our estimate of the relative contribution to high-$O_3$ events. The results are reported in Figure S8a for all AQS sites within the same region used in Figure 10, suggesting no direct relationship ($r^2$ = 0.02) between Asian enhancements and model bias in surface $O_3$. *Reidmiller et al.* [2009] found an anti-correlation between foreign influence and model biases for a 15-model average (year 2001), and thus suggested that global models may underestimate foreign contribution. We do not find any evidence for this relationship in our model.

[43] Next we explore the influence of Asian emissions on high-$O_3$ episodes at three representative CASTNet sites (Figure 11). Episodes of elevated $O_3$ mixing ratios are observed at the national park ground stations, lagged by 1–2 days after the onset of Asian pollution events over the U.S. west coast discussed in section 3 (gray shaded periods in Figure 11). During these events from May–June 2010, surface $O_3$ anomalies of up to +15 ppbv are observed at the three sites, with the model attributing approximately 2–9 ppbv positive anomalies to Asian anthropogenic emissions. The GFDL AM3 high-resolution model captures 45–65% of observed day-to-day variability of surface $O_3$ at the ground stations, and the Asian anthropogenic enhancements can explain 25–30% of the variability in the model total $O_3$. The results indicate that subsiding Asian pollution directly contributes to some high-$O_3$ episodes at the CASTNet stations in the mountain west, consistent with our findings in section 3 and Figure 10.

## 6. Forecasting Asian Pollution Events in the Western U.S. From Space

[44] In this section we explore the potential to develop a space-based indicator for Asian pollution enhancements to surface $O_3$ over the western USA. The method involves the correlation of daily AIRS CO columns at each 1° × 1° grid box with the Asian contribution to MDA8 $O_3$ in the model

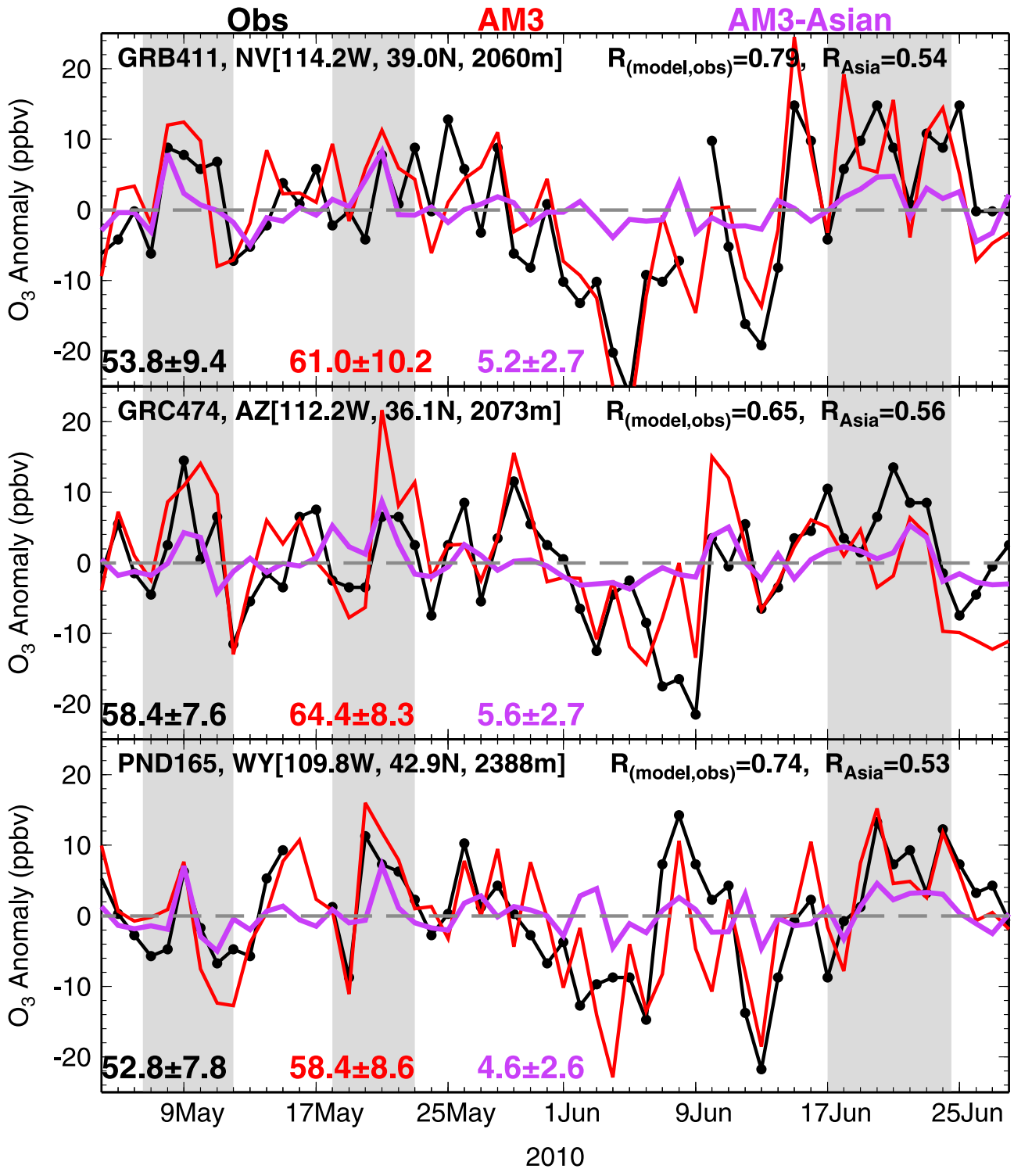


**Figure 11.** Day-to-day variability of observed (black), modeled (red) and Asian enhancements (purple) to daily maximum 8-h average ozone at three CASTNet surface stations (triangles in Figure 9a). Shown are anomalies relative to the May–June mean. The gray shading indicates major Asian pollution events discussed in section 3.

surface layer for western U.S. national parks, for time lags of 0 to 3 days between the data sets. Figure 12 shows an example for Grand Canyon National Park. The region with the greatest correlation over the eastern North Pacific represents the region from which air is preferentially transported to the U.S. west coast lower troposphere within the time lag (transport time to the high elevation receptor site) indicated. In Figure 12 strong correlations emerge with

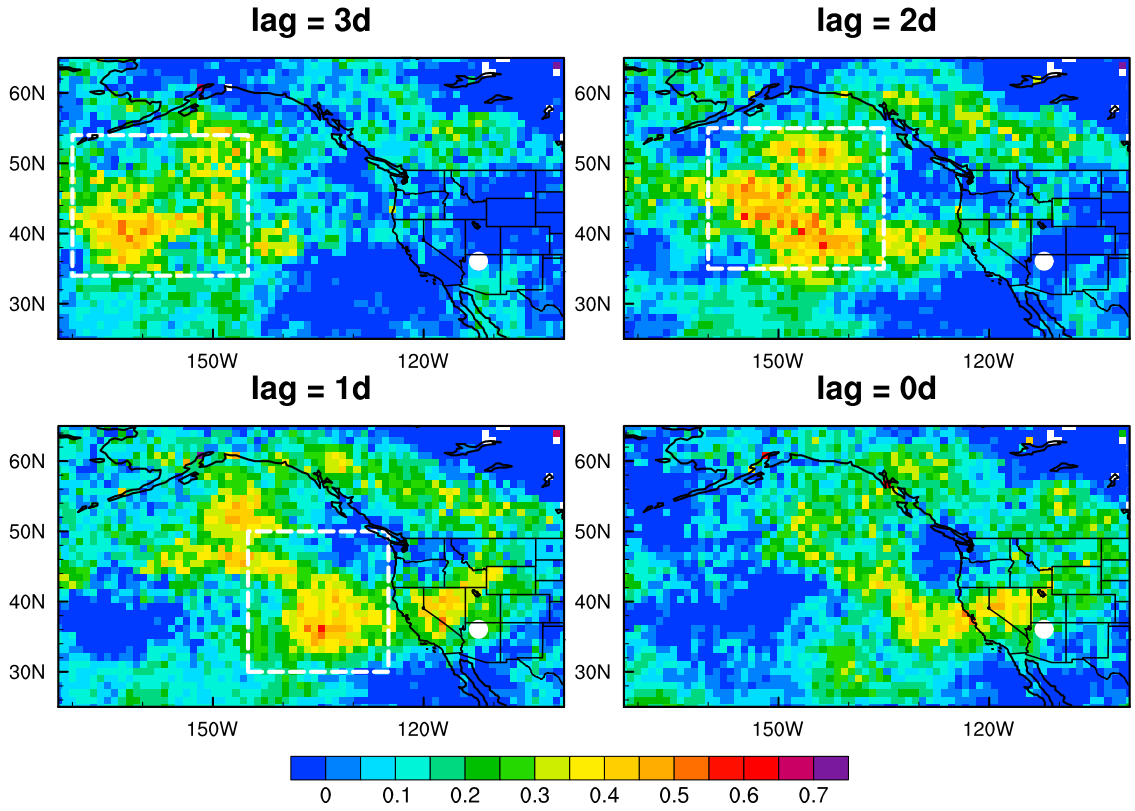


**Figure 12.** Correlation coefficients between May–June 2010 AIRS daily CO columns at each 1° × 1° grid box and AM3 estimated Asian anthropogenic enhancements to daily maximum 8-h average ozone at Grand Canyon National Park (denoted as a white circle), Arizona, considering time lags of 0–3 days. The rectangles indicate the regions where AIRS CO can be used to derive a space-spaced indicator of Asian influence on surface ozone in the western U.S. (section 6).

AIRS CO columns over approximately 30°–50°N of the northeast Pacific; the region that gives the best correlation with the surface data shifts from west to east as the time offset decreases, reflecting the progression of Asian pollution toward the U.S. west coast consistent with Figure 1. Correlation results for other ground stations in the western mountains show a similar large-scale feature, with the region experiencing the peak correlation falling within the boxes denoted in Figure 12.

[45] Based on the correlation analysis, we hypothesize that variability of AIRS CO measurements averaged over the eastern North Pacific within these boxes can serve at least as a qualitative warning index to inform regional air quality management decisions about incoming Asian enhancements to surface $O_3$ in the western mountains. Figure 13 elaborates on this hypothesis by illustrating a time series of AIRS CO averaged over the eastern North Pacific between 30°–50°N latitudes and 145°–125°W longitudes (box in lag = 1d panel of Figure 12), together with Asian enhancements to surface MDA8 $O_3$ averaged over Great Basin, Grand Canyon and Canyonlands National Parks. The variability in AIRS CO is confounded by the seasonal increase in OH, which leads to a decreasing trend ($-6.1 \times 10^{15}$ molecules/cm$^2$ per day, $r^2$ = 0.74) in CO from May to June. To highlight the CO variability due to trans-Pacific transport, we remove the linear trend from the time series of AIRS CO, which more clearly shows the three major trans-Pacific Asian pollution events discussed in section 3 (May 7–12, May 17–22, and June 17–22). Further supporting the utility of satellite-based CO column measurements as an early warning indicator for surface air quality, we find that the timing of peak Asian enhancements on surface $O_3$ over the Rocky Mountains generally appears 1–3 days later than the peak AIRS CO off the U.S. west coast. Generalizing from the analysis in section 3 and Figures 12 and 13, we find that it takes approximately 3–6 days for the Asian pollution plumes arriving over the eastern North Pacific, which can be detected from space, to be transported into western U.S. surface air during the late spring and early summer of 2010.

[46] We note that the relationship between AIRS CO and Asian $O_3$ pollution events in the western U.S. shown here is qualitatively promising in terms of daily to synoptic-scale variability. The $\Delta O_3$ due to Asian influence may not have a quantitative relationship with $\Delta$CO represented by AIRS since Asian pollution transported to the eastern North Pacific may not consistently reach the same locations given variability in meteorological conditions. Future work should explore the interannual variability in the vertical extent of Asian pollution over the U.S. west coast as well as explore whether retrievals at particular levels (rather than the total column) contain a more quantitative relationship with the Asian surface $O_3$ over the U.S. Mountain West. The correlation between satellite-detected CO enhancements over the eastern North Pacific and the Asian pollution reaching

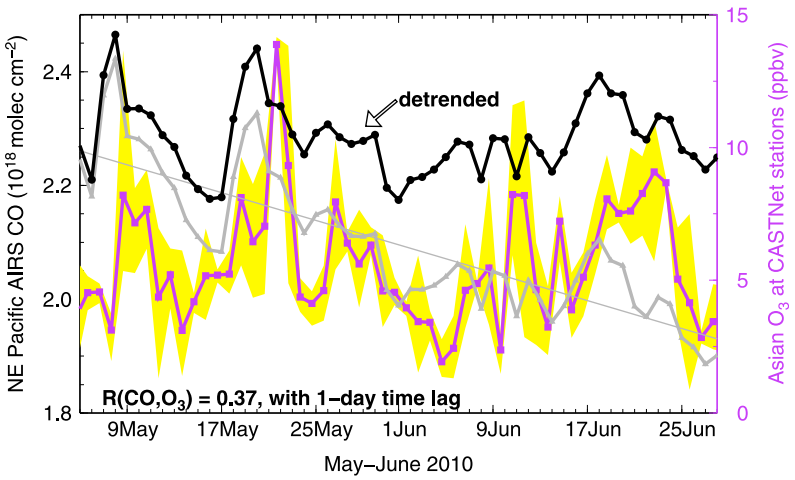


**Figure 13.** Time series illustrating increasing Asian enhancements to surface ozone (purple) at CASTNet sites following 1–2 days after peak CO columns represented by AIRS (gray, detrended in black) over the eastern North Pacific (30°–50°N, 145°–125°W). The yellow shading indicates the range of Asian enhancements at the three sites: Great Basin, Grand Canyon, and Canyonlands National Parks.

western U.S. surface air should be further examined using multiyear data sets.

## 7. Conclusions

[47] We have applied a new high-resolution (~50 × 50 km$^2$) global chemistry-climate model (GFDL AM3) to examine the transport pathways of Asian pollution over the western U.S. in spring 2010, with a primary focus on the influence of Asian pollution on surface $O_3$ air quality. To the best of our knowledge, this is the first time a global high-resolution model with full stratospheric and tropospheric chemistry has been employed to address the problem of trans-Pacific pollution transport.

[48] Extensive observations during the CalNex field campaign (May–June 2010) enable a process-oriented assessment of the model in simulating regional transport and chemistry over the western USA. Evaluation with surface $O_3$ networks shows that the model captures much of the observed day-to-day variability in daily maximum 8-h average $O_3$ (MDA8) in surface air, with correlation coefficients ranging from 0.4 to 0.8 and simulated standard deviations within 15% of those observed for most sites. The most severe limitation for our study is a high surface $O_3$ bias of 2–10 ppbv on average in the high elevation regions and up to 10–25 ppbv at the Pacific coastal sites (section 4). The model bias in surface $O_3$ does not have a direct relationship with the Asian enhancement.

[49] An integrated analysis of satellite measurements of CO and total $O_3$ columns from AIRS, ozonesondes, and model diagnostics reveals two cases of interleaving and mixing of Asian pollution with stratospheric air associated with complex airstream interactions as midlatitude cyclones cross the North American west coast during CalNex (May 17–20 and June 17–19) - a transport mechanism noted by prior studies [e.g., *Stohl and Trickl* 1999; *Cooper et al.*, 2004b]. The GFDL AM3 model successfully reproduces the prominent features of these events, and implies that transported stratospheric remnants from a deep tropopause fold may contribute 50–60% of distinct $O_3$ layers between 2 and 4 km above the California coast. Asian pollution, arriving a day after deep tropopause folding, contributes 20–30% of total $O_3$ in the mid-troposphere when the air was sampled by the ozonesondes (section 3.1). We note our estimates should be viewed as upper limits as discussed in section 2.4.

[50] Using both the model and observations, we further illustrate that Asian pollution over the U.S. west coast descends isentropically behind cold fronts toward the south (sections 3.2 and 3.3), consistent with prior model studies [*Cooper et al.*, 2011; *Brown-Steiner and Hess* 2011]. Combined with the influence of additional $O_3$ produced from the thermal decomposition of Asian PAN during subsidence, the Asian enhancement to $O_3$ at ~800 hPa exhibits a pronounced maximum in the southwestern U.S. (including parts of California, Nevada, Utah, and Arizona; section 5.1). We find that the Asian enhancement in the model surface layer over this region increases for total MDA8 $O_3$ concentrations in the 70–90 ppbv range compared with that in the 60–70 ppbv range (Figure 10). We estimate that in the absence of Asian anthropogenic emissions, 49% of springtime MDA8 $O_3$ exceedances of 70 ppbv in the model would not have occurred over the southwestern U.S. For a 60 ppbv or 75 ppbv threshold, that statistic is 20% or 53%, respectively (section 5.2).

[51] During strong trans-Pacific transport events, the Asian enhancement to MDA8 $O_3$ in western U.S. surface air can reach 8–15 ppbv in high-elevation regions experiencing peak surface $O_3$ levels in excess of 60 ppbv (Figures 6 and 8). We further demonstrate the potential for using near real-time satellite measurements of CO columns (AIRS) over the eastern North Pacific at daily intervals to develop space-based criteria to identify these strong Asian pollution events (Figures 12 and 13). Such a space-based index could serve as an early warning indicator (lead time of 1–3 days) for the potential influence of Asian pollution on surface $O_3$ air quality and any associated health advisories for National Park Services.

[52] Our analysis suggests that consideration of enhancements from Asian anthropogenic emissions will be important to develop effective $O_3$ abatement strategies for the western

USA. There is a high degree of uncertainty regarding the trend of Asian emissions over the next few decades. The RCP (Representative Concentration Pathways) scenarios for IPCC Fifth Assessment Report [*Moss et al.*, 2010] indicate that East Asian $NO_x$ emissions peak in 2020–2040 with ~10–30% increase from 2010 levels. It therefore seems likely that the Asian component of U.S. baseline $O_3$ will continue to increase at least in the coming decade, although coincident reductions in other northern hemispheric source regions may cancel such increases, with little change in baseline $O_3$ over North America. Constant baseline $O_3$ would make $O_3$ abatement more difficult under more stringent NAAQS, and increasing baseline would further confound $O_3$ abatement efforts (the "tightening vise" of *Keating et al.* [2004]).

[53] **Acknowledgments.** This work is supported by the Cooperative Institute for Climate Science (CICS), a collaboration between Princeton University and NOAA Geophysical Fluid Dynamics Laboratory (GFDL). The satellite data analysis is funded by the NASA Air Quality Applied Science Team (AQAST) (NNH09ZDA001N). Funding for the IONS-2010 field campaign was provided by NOAA ESRL Health of the Atmosphere Program, NASA Tropospheric Chemistry Program, U.S. Navy, Environment Canada, and NOAA's National Air Quality Forecast Capability. We acknowledge the free use of tropospheric $NO_2$ column data from the SCIAMACHY sensor from www.tenis.nl and Bahreini Roya at NOAA ESRL for help collecting the AMS aerosol measurements onboard the WP-3D aircraft. We are grateful to Songmiao Fan and Hiram Levy II at NOAA GFDL and Pat Dolwick at EPA for helpful comments in improving an earlier version of this manuscript.

## References

Ambrose, J. L., D. R. Reidmiller, and D. A. Jaffe (2011), Causes of high $O_3$ in the lower free troposphere over the Pacific Northwest as observed at the Mt. Bachelor Observatory, *Atmos. Environ.*, *45*, 5302–5315, doi:10.1016/j.atmosenv.2011.06.056.

Aumann, H. H., et al. (2003), AIRS/AMSU/HSB on the Aqua mission: Design, science objectives, data products, and processing systems, *IEEE Trans. Geosci. Remote Sens.*, *41*, 253–264, doi:10.1109/TGRS.2002.808356.

Austin, J., and R. J. Wilson (2006), Ensemble simulations of the decline and recovery of stratospheric ozone, *J. Geophys. Res.*, *111*, D16314, doi:10.1029/2005JD006907.

Austin, J., and R. J. Wilson (2010), Sensitivity of polar ozone to sea surface temperatures and halogen amounts, *J. Geophys. Res.*, *115*, D18303, doi:10.1029/2009JD013292.

Bahreini, R., et al. (2009), Organic aerosol formation in urban and industrial plumes near Houston and Dallas, Texas, *J. Geophys. Res.*, *114*, D00F16, doi:10.1029/2008JD011493 [printed 115(D7), 2010].

Boersma, K. F., H. J. Eskes, and E. J. Brinksma (2004), Error analysis for tropospheric $NO_2$ retrieval from space, *J. Geophys. Res.*, *109*, D04311, doi:10.1029/2003JD003962.

Brock, C. A., et al. (2004), Particle characteristics following cloud-modified transport from Asia to North America, *J. Geophys. Res.*, *109*, D23S26, doi:10.1029/2003JD004198.

Brown-Steiner, B., and P. Hess (2011), Asian influence on surface ozone in the United States: A comparison of chemistry, seasonality, and transport mechanisms, *J. Geophys. Res.*, *116*, D17309, doi:10.1029/2011JD015846.

Burk, S. D., and W. T. Thompson (1996), The summertime low-level jet and marine boundary layer structure along the California coast, *Mon. Weather Rev.*, *124*, 668–686, doi:10.1175/1520-0493(1996)124<0668:TSLLJA>2.0.CO;2.

Carmichael, G. R., et al. (2003), Regional-scale chemical transport modeling in support of the analysis of observations obtained during the TRACE-P experiment, *J. Geophys. Res.*, *108*(D21), 8823, doi:10.1029/2002JD003117.

Chen, G., et al. (2005), An investigation of the chemistry of ship emission plumes during ITCT 2002, *J. Geophys. Res.*, *110*, D10S90, doi:10.1029/2004JD005236.

Chen, Y., C. Zhao, Q. Zhang, Z. Deng, M. Huang, and X. Ma (2009), Aircraft study of mountain chimney effect of Beijing, China, *J. Geophys. Res.*, *114*, D08306, doi:10.1029/2008JD010610.

Chin, M., T. Diehl, P. Ginoux, and W. Malm (2007), Intercontinental transport of pollution and dust aerosols: Implications for regional air quality, *Atmos. Chem. Phys.*, *7*, 5501–5517, doi:10.5194/acp-7-5501-2007.

Cooper, O. R., et al. (2004a), A case study of transpacific warm conveyor belt transport: Influence of merging airstreams on trace gas import to North America, *J. Geophys. Res.*, *109*, D23S08, doi:10.1029/2003JD003624.

Cooper, O. R., et al. (2004b), On the life cycle of a stratospheric intrusion and its dispersion into polluted warm conveyor belts, *J. Geophys. Res.*, *109*, D23S09, doi:10.1029/2003JD004006.

Cooper, O. R., et al. (2010), Increasing springtime ozone mixing ratios in the free troposphere over western North America, *Nature*, *463*, 344–348, doi:10.1038/nature08708.

Cooper, O. R., et al. (2011), Measurement of western U.S. baseline ozone from the surface to the tropopause and assessment of downwind impact regions, *J. Geophys. Res.*, *116*, D00V03, doi:10.1029/2011JD016095.

Dentener, F., et al. (2006), Emissions of primary aerosol and precursor gases in the years 2000 and 1750 prescribed datasets for AeroCom, *Atmos. Chem. Phys.*, *6*, 4321–4344, doi:10.5194/acp-6-4321-2006.

Ding, A., et al. (2009), Transport of north China air pollution by midlatitude cyclones: Case study of aircraft measurements in summer 2007, *J. Geophys. Res.*, *114*, D08304, doi:10.1029/2008JD011023.

Donner, L. J., et al. (2011), The dynamical core, physical parameterizations, and basic simulation characteristics of the atmospheric component AM3 of the GFDL Global Coupled Model CM3, *J. Clim.*, *24*, 3484–3519, doi:10.1175/2011JCLI3955.1.

Drewnick, F., et al. (2005), A new time-of-flight aerosol mass spectrometer (TOF-AMS)- Instrument description and first field deployment, *Aerosol Sci. Technol.*, *39*(7), 637–658, doi:10.1080/02786820500182040.

Dunlea, E. J., et al. (2009), Evolution of Asian aerosols during transpacific transport in INTEX-B, *Atmos. Chem. Phys.*, *9*, 7257–7287, doi:10.5194/acp-9-7257-2009.

Edwards, D. P., et al. (2003), Tropospheric ozone over the tropical Atlantic: A satellite perspective, *J. Geophys. Res.*, *108*(D8), 4237, doi:10.1029/2002JD002927.

Emmons, L. K., et al. (2010), Description and evaluation of the Model for Ozone and Related chemical Tracers, version 4 (MOZART-4), *Geosci. Model Dev.*, *3*, 43–67, doi:10.5194/gmd-3-43-2010.

Environmental Protection Agency (2010), National ambient air quality standards for ozone, *Fed. Regist.*, *75*(11), 2938–3052.

Esler, J. G., P. H. Haynes, K. S. Law, H. Barjat, K. Dewey, J. Kent, S. Schmitgen, and N. Brough (2003), Transport and mixing between airmasses in cold frontal regions during Dynamics and Chemistry of Frontal Zones (DCFZ), *J. Geophys. Res.*, *108*(D4), 4142, doi:10.1029/2001JD001494.

Ewing, S. A., et al. (2010), Pb Isotopes as an indicator of the Asian contribution to particulate air pollution in urban California, *Environ. Sci. Technol.*, *44*(23), 8911–8916, doi:10.1021/es101450t.

Fang, Y., A. M. Fiore, L. W. Horowitz, A. Gnanadesikan, I. Held, G. Chen, G. Vecchi, and H. Levy (2011), The impacts of changing transport and precipitation on pollutant distributions in a future climate, *J. Geophys. Res.*, *116*, D18303, doi:10.1029/2011JD015642.

Felker, S. R., J. L. Moody, A. J. Wimmers, G. Osterman, and K. Bowman (2011), A multi-sensor upper tropospheric ozone product (MUTOP) based on TES ozone and GOES water vapor: Derivation, *Atmos. Chem. Phys.*, *11*, 6515–6527, doi:10.5194/acp-11-6515-2011.

Fiore, A. M., D. J. Jacob, I. Bey, R. M. Yantosca, B. D. Field, A. C. Fusco, and J. G. Wilkinson (2002), Background ozone over the United States in summer: Origin, trend, and contribution to pollution episodes, *J. Geophys. Res.*, *107*(D15), 4275, doi:10.1029/2001JD000982.

Fischer, E. V., D. A. Jaffe, D. R. Reidmiller, and L. Jaegle (2010), Meteorological controls on observed peroxyacetyl nitrate at Mount Bachelor during the spring of 2008, *J. Geophys. Res.*, *115*, D03302, doi:10.1029/2009JD012776.

Fischer, E. V., D. A. Jaffe, and E. C. Weatherhead (2011), Free tropospheric peroxyacetyl nitrate (PAN) and ozone at Mount Bachelor: Potential causes of variability and timescale for trend detection, *Atmos. Chem. Phys.*, *11*, 5641–5654, doi:10.5194/acp-11-5641-2011.

Golaz, J.-C., M. Salzmann, L. J. Donner, L. W. Horowitz, Y. Ming, and M. Zhao (2011), Sensitivity of the aerosol indirect effect to subgrid variability in the cloud parameterization of the GFDL Atmosphere General Circulation Model AM3, *J. Clim.*, *24*, 3145–3160, doi:10.1175/2010JCLI3945.1.

Goldstein, A. H., et al. (2004), Impact of Asian emissions on observations at Trinidad Head, California, during ITCT 2K2, *J. Geophys. Res.*, *109*, D23S17, doi:10.1029/2003JD004406.

Griffies, S. M., et al. (2011), GFDL's CM3 Coupled Climate Model: Characteristics of the ocean and sea ice simulations, *J. Clim.*, *24*, 3520–3544, doi:10.1175/2011JCLI3964.1.

Guenther, A., T. Karl, P. Harley, C. Wiedinmyer, P. Palmer, and C. Geron (2006), Estimates of global terrestrial isoprene emissions using MEGAN (Model of Emissions of Gases and Aerosols from Nature), *Atmos. Chem. Phys.*, *6*, 3181–3210, doi:10.5194/acp-6-3181-2006.

Heald, C. L., et al. (2003), Asian outflow and transpacific transport of carbon monoxide and ozone pollution: An integrated satellite, aircraft and model perspective, *J. Geophys. Res.*, *108*(D24), 4804, doi:10.1029/2003JD003507.

Holloway, J., R. Jakoubek, D. Parrish, C. Gerbig, A. Volz-Thomas, S. Schmitgen, A. Fried, B. Wert, B. Henry, and J. Drummond (2000), Airborne intercomparison of vacuum ultraviolet fluorescence and tunable diode laser absorption measurements of tropospheric carbon monoxide, *J. Geophys. Res.*, *105*(D19), 24,251–24,261, doi:10.1029/2000JD900237.

Horowitz, L. W., et al. (2003), A global simulation of tropospheric ozone and related tracers: Description and evaluation of MOZART, version 2, *J. Geophys. Res.*, *108*(D24), 4784, doi:10.1029/2002JD002853.

Horowitz, L. W., et al. (2007), Observational constraints on the chemistry of isoprene nitrates over the eastern Unites States, *J. Geophys. Res.*, *112*, D12S08, doi:10.1029/2006JD007747.

Huang, M., et al. (2010), Impacts of transported background ozone on California air quality during the ARCTAS-CARB period a multi-scale modeling study, *Atmos. Chem. Phys.*, *10*, 6947–6968, doi:10.5194/acp-10-6947-2010.

Hudman, R. C., et al. (2004), Ozone production in transpacific Asian pollution plumes and implications for ozone air quality in California, *J. Geophys. Res.*, *109*, D23S10, doi:10.1029/2004JD004974.

Husar, R., et al. (2001), Asian dust events of April 1998, *J. Geophys. Res.*, *106*(D16), 18,317–18,330, doi:10.1029/2000JD900788.

Jacob, D. J., J. A. Logan, and P. P. Murti (1999), Effect of rising Asian emissions on surface ozone in the United States, *Geophys. Res. Lett.*, *26*, 2175–2178, doi:10.1029/1999GL900450.

Jaeglé, L., et al. (2003), Sources and budgets for CO and $O_3$ in the northeastern Pacific during the spring of 2001: Results from the PHOBEA-II Experiment, *J. Geophys. Res.*, *108*(D20), 8802, doi:10.1029/2002JD003121.

Jaffe, D. A., et al. (1999), Transport of Asian air pollution to North America, *Geophys. Res. Lett.*, *26*, 711–714, doi:10.1029/1999GL900100.

Jaffe, D. A., D. Parrish, A. Goldstein, H. Price, and J. Harris (2003a), Increasing background ozone during spring on the west coast of North America, *Geophys. Res. Lett.*, *30*(12), 1613, doi:10.1029/2003GL017024.

Jaffe, D., J. Snow, and O. Cooper (2003b), The 2001 Asian dust events: Transport and impact on surface aerosol concentrations in the U.S, *Eos Trans. AGU*, *84*(46), 501, doi:10.1029/2003EO460001.

Jonson, J. E., et al. (2010), A multi-model analysis of vertical ozone profiles, *Atmos. Chem. Phys.*, *10*, 5759–5783, doi:10.5194/acp-10-5759-2010.

Kanamitsu, M., et al. (1991), Recent changes implemented into the global forecast system at NMC, *Weather Forecast.*, *6*, 425–435, doi:10.1175/1520-0434(1991)006<0425:RCIITG>2.0.CO;2.

Keating, T. J., J. J. West, and A. E. Farrell (2004), Prospects for international management of the intercontinental air pollution transport, in *Intercontinental Transport of Air Pollution*, edited by A. Stohl, pp. 295–320, Springer, Berlin.

Kleinman, L., et al. (1994), Ozone formation at a rural site in the southeastern United States, *J. Geophys. Res.*, *99*(D2), 3469–3482, doi:10.1029/93JD02991.

Knutson, T. R., J. J. Sirutis, S. T. Garner, G. A. Vecchi, and I. Held (2008), Simulated reduction in Atlantic hurricane frequency under twenty-first-century warming conditions, *Nat. Geosci.*, *1*(6), 359–364, doi:10.1038/ngeo202.

Koumoutsaris, S., I. Bey, S. Generoso, and V. Thouret (2008), Influence of El Nino-Southern Oscillation on the interannual variability of tropospheric ozone in the northern mid-latitudes, *J. Geophys. Res.*, *113*, D19301, doi:10.1029/2007JD009753.

Lamarque, J.-F., et al. (2010), Historical (1850–2000) gridded anthropogenic and biomass burning emissions of reactive gases and aerosols: Methodology and application, *Atmos. Chem. Phys.*, *10*, 7017–7039, doi:10.5194/acp-10-7017-2010.

Lamsal, L. N., R. V. Martin, A. Padmanabhan, A. van Donkelaar, Q. Zhang, C. E. Sioris, K. Chance, T. P. Kurosu, and M. J. Newchurch (2011), Application of satellite observations for timely updates to global anthropogenic NOx emission inventories, *Geophys. Res. Lett.*, *38*, L05810, doi:10.1029/2010GL046476.

Langford, A. O., C. J. Senff, R. J. Alvarez, R. M. Banta, and R. M. Hardesty (2010), Long-range transport of ozone from the Los Angeles Basin: A case study, *Geophys. Res. Lett.*, *37*, L06807, doi:10.1029/2010GL042507.

Langford, A. O., J. Brioude, O. R. Cooper, C. J. Senff, R. J. Alvarez II, R. M. Hardesty, B. J. Johnson, and S. J. Oltmans (2011), Stratospheric influence on surface ozone in the Los Angeles area during late spring and early summer of 2010, *J. Geophys. Res.*, *117*, D00V06, doi:10.1029/2011JD016766.

Lefohn, A. S., D. S. Shadwick, and S. D. Ziman (1998), The difficult challenge of attaining EPA's new ozone standard, *Environ. Sci. Technol.*, *32*, 276A–282A, doi:10.1021/es983569x.

Lei, Y., Q. Zhang, K. B. He, and D. G. Streets (2011), Primary anthropogenic aerosol emission trends for China, 1990–2005, *Atmos. Chem. Phys.*, *11*, 931–954, doi:10.5194/acp-11-931-2011.

Li, F., P. Ginoux, and V. Ramaswamy (2010), Transport of Patagonian dust to Antarctica, *J. Geophys. Res.*, *115*, D18217, doi:10.1029/2009JD012356.

Liang, Q., L. Jaegle, and J. M. Wallace (2005), Meteorological indices for Asian outflow and transpacific transport on daily to interannual timescales, *J. Geophys. Res.*, *110*, D18308, doi:10.1029/2005JD005788.

Liang, Q., et al. (2007), Summertime influence of Asian pollution in the free troposphere over North America, *J. Geophys. Res.*, *112*, D12S11, doi:10.1029/2006JD007919.

Lin, J.-T., and M. B. McElroy (2011), Detection from space of a reduction in anthropogenic emissions of nitrogen oxides during the Chinese economic downturn, *Atmos. Chem. Phys. Discuss.*, *11*, 193–223, doi:10.5194/acpd-11-193-2011.

Lin, M., T. Holloway, T. Oki, D. G. Streets, and A. Richter (2009), Multi-scale model analysis of boundary layer ozone over East Asia, *Atmos. Chem. Phys.*, *9*, 3277–3301, doi:10.5194/acp-9-3277-2009.

Lin, M., T. Holloway, G. R. Carmichael, and A. M. Fiore (2010), Quantifying pollution inflow and outflow over East Asia in spring with regional and global models, *Atmos. Chem. Phys.*, *10*, 4221–4239, doi:10.5194/acp-10-4221-2010.

Liu, H. Y., et al. (2003), Transport pathways for Asian pollution outflow over the Pacific: Interannual and seasonal variations, *J. Geophys. Res.*, *108*(D20), 8786, doi:10.1029/2002JD003102.

Liu, J., D. L. Mauzerall, and L. W. Horowitz (2005), Analysis of seasonal and interannual variability in transpacific transport, *J. Geophys. Res.*, *110*, D04302, doi:10.1029/2004JD005207.

Lu, Z., D. G. Streets, Q. Zhang, S. Wang, G. R. Carmichael, Y. F. Cheng, C. Wei, M. Chin, T. Diehl, and Q. Tan (2010), Sulfur dioxide emissions in China and sulfur trends in East Asia since 2000, *Atmos. Chem. Phys.*, *10*, 6311–6331, doi:10.5194/acp-10-6311-2010.

McKendry, G., et al. (2008), Trans-Pacific dust events observed at Whistler, British Columbia during INTEX-B, *Atmos. Chem. Phys.*, *8*, 6297–6307, doi:10.5194/acp-8-6297-2008.

McMillan, W. W., et al. (2005), Daily global maps of carbon monoxide from NASA's Atmospheric Infrared Sounder, *Geophys. Res. Lett.*, *32*, L11801, doi:10.1029/2004GL021821.

McMillan, W. W., et al. (2008), AIRS views transport from 12 to 22 July 2004 Alaskan/Canadian fires: Correlation of AIRS CO and MODIS AOD with forward trajectories and comparison of AIRS CO retrievals with DC-8 in situ measurements during INTEX-A/ICARTT, *J. Geophys. Res.*, *113*, D20301, doi:10.1029/2007JD009711.

McMillan, W. W., K. D. Evans, C. D. Barnet, E. S. Maddy, G. W. Sachse, and G. S. Diskin (2011), Validating the AIRS Version 5 CO Retrieval With DACOM In Situ Measurements During INTEX-A and -B, *IEEE Trans. Geosci. Remote Sens.*, *49*(7), 2802–2813, doi:10.1109/TGRS.2011.2106505.

Moss, R. H., et al. (2010), The next generation of scenarios for climate change research and assessment, *Nature*, *463*, 747–756, doi:10.1038/nature08823.

Moxim, W., H. Levy II, and P. Kasibhatla (1996), Simulated global tropospheric PAN: Its transport and impact on NOx, *J. Geophys. Res.*, *101*(D7), 12,621–12,638, doi:10.1029/96JD00338.

Neuman, J. A., et al. (2012), Observations of ozone transport from the free troposphere to the Los Angeles basin, *J. Geophys. Res.*, doi:10.1029/2011JD016919, in press.

Ohara, T., H. Akimoto, J. Kurokawa, N. Horii, K. Yamaji, X. Yan, and T. Hayasaka (2007), An Asian emission inventory of anthropogenic emission sources for the period 1980–2020, *Atmos. Chem. Phys.*, *7*, 4419–4444, doi:10.5194/acp-7-4419-2007.

Oltmans, S. J., A. S. Lefohn, J. M. Harris, and D. S. Shadwick (2008), Background ozone levels of air entering the west coast of the U.S. and assessment of longer-term changes, *Atmos. Environ.*, *42*, 6020–6038, doi:10.1016/j.atmosenv.2008.03.034.

Pan, L. L., et al. (2007), Chemical behavior of the tropopause observed during the Stratosphere-Troposphere Analyses of Regional Transport (START) experiment, *J. Geophys. Res.*, *112*, D18110, doi:10.1029/2007JD008645.

Parish, T. R. (2000), Forcing of the summertime low-level jet along the California coast, *J. Appl. Meteorol.*, *39*, 2421–2433, doi:10.1175/1520-0450(2000)039<2421:FOTSLL>2.0.CO;2.

Parrish, D., J. Holloway, R. Jakoubek, M. Trainer, T. Ryerson, G. Hübler, F. Fehsenfeld, J. Moody, and O. Cooper (2000), Mixing of anthropogenic pollution with stratospheric ozone: A case study from the North Atlantic wintertime troposphere, *J. Geophys. Res.*, *105*(D19), 24,363–24,374, doi:10.1029/2000JD900291.

Parrish, D. D., D. B. Millet, and A. H. Goldstein (2009), Increasing ozone in marine boundary layer inflow at the west coasts of North America and Europe, *Atmos. Chem. Phys.*, *9*, 1303–1323, doi:10.5194/acp-9-1303-2009.

Parrish, D. D., K. C. Aikin, S. J. Oltmans, B. J. Johnson, M. Ives, and C. Sweeny (2010), Impact of transported background ozone inflow on summertime air quality in a California ozone exceedance area, *Atmos. Chem. Phys.*, *10*, 10,093–10,109, doi:10.5194/acp-10-10093-2010.

Peltier, R. E., A. H. Hecobian, R. J. Weber, A. Stohl, E. L. Atlas, D. D. Riemer, D. R. Blake, E. Apel, T. Campos, and T. Karl (2008), Investigating the sources and atmospheric processing of fine particles from Asia and the Northwestern United States measured during INTEX B, *Atmos. Chem. Phys.*, *8*, 1835–1853, doi:10.5194/acp-8-1835-2008.

Pfister, G. G., et al. (2011), Characterizing summertime chemical boundary conditions for airmasses entering the US West Coast, *Atmos. Chem. Phys.*, *11*, 1769–1790, doi:10.5194/acp-11-1769-2011.

Pittman, J. V., et al. (2009), Evaluation of AIRS, IASI, and OMI ozone profile retrievals in the extratropical tropopause region using in situ aircraft measurements, *J. Geophys. Res.*, *114*, D24109, doi:10.1029/2009JD012493.

Putman, W. M., and S.-J. Lin (2007), Finite-volume transport on various cubed-sphere grid, *J. Comput. Phys.*, *227*, 55–78, doi:10.1016/j.jcp.2007.07.022.

Rasmussen, D. J., A. M. Fiore, V. Naik, L. W. Horowitz, S. J. McGinnis, and M. G. Schultz (2011), Surface ozone-temperature relationships in the eastern US: A monthly climatology for evaluating chemistry-climate models, *Atmos. Environ.*, *47*, 142–153, doi:10.1016/j.atmosenv.2011.11.021.

Rastigejev, Y., R. Park, M. P. Brenner, and D. J. Jacob (2010), Resolving intercontinental pollution plumes in global models of atmospheric transport, *J. Geophys. Res.*, *115*, D02302, doi:10.1029/2009JD012568.

Reidmiller, D. R., et al. (2009), The influence of foreign vs. North American emissions on surface ozone in the US, *Atmos. Chem. Phys.*, *9*, 5027–5042, doi:10.5194/acp-9-5027-2009.

Richter, A., et al. (2005), Increase in tropospheric nitrogen dioxide over China observed from space, *Nature*, *437*(7055), 129–132, doi:10.1038/nature04092.

Ryerson, T., et al. (1998), Emissions lifetimes and ozone formation in power plant plumes, *J. Geophys. Res.*, *103*(D17), 22,569–22,583, doi:10.1029/98JD01620.

Skamarock, W. C., J. B. Klemp, J. Dudhia, D. O. Gill, D. M. Barker, M. G. Duda, X.-Y. Huang, W. Wang, and J. G. Powers (2008), A description of the advanced research WRF version 3, *NCAR Tech. Note NCAR/TN–475+STR*, Natl. Cent. for Atmos. Res, Boulder, Colo.

Stohl, A., and T. Trickl (1999), A textbook example of long-range transport: Simultaneous observation of ozone maxima of stratospheric and North American origin in the free troposphere over Europe, *J. Geophys. Res.*, *104*, 30,445–30,462, doi:10.1029/1999JD900803.

Stohl, A., et al. (2007), Arctic smoke record air pollution levels in the European Arctic during a period of abnormal warmth, due to agricultural fires in eastern Europe, *Atmos. Chem. Phys.*, *7*, 511–534, doi:10.5194/acp-7-511-2007.

Susskind, J., C. D. Barnet, and J. M. Blaisdell (2003), Retrieval of atmospheric and surface parameters from AIRS/AMSU/HSB data in the presence of clouds, *IEEE Trans. Geosci. Remote Sens.*, *41*, 390–409, doi:10.1109/TGRS.2002.808236.

Tanimoto, H., Y. Sawa, H. Matsueda, I. Uno, T. Ohara, K. Yamaji, J. Kurokawa, and S. Yonemura (2005), Significant latitudinal gradient in the surface ozone spring maximum over East Asia, *Geophys. Res. Lett.*, *32*, L21805, doi:10.1029/2005GL023514.

Task Force on Hemispheric Transport of Air Pollution (TFHTAP) (2011), *Hemispheric Transport of Air Pollution 2010, Part A: Ozone and Particulate Matter*, *Air Pollut. Stud.*, vol. 17, U. N. Econ. Comm. Eur., Geneva, Switzerland.

Trainer, M., et al. (1993), Correlations of ozone with NOx in photochemically aged air, *J. Geophys. Res.*, *98*, 2917–2925, doi:10.1029/92JD01910.

Uno, I., et al. (2009), Asian dust transported one full circuit around the globe, *Nat. Geosci.*, *2*, 557–560, doi:10.1038/ngeo583.

Val Martin, M., J. A. Logan, R. A. Kahn, F.-Y. Leung, D. L. Nelson, and D. J. Diner (2010), Smoke injection heights from fires in North America: Analysis of 5 years of satellite observations, *Atmos. Chem. Phys.*, *10*, 1491–1510, doi:10.5194/acp-10-1491-2010.

van Noije, T., H. Eskes, M. van Weele, and P. van Velthoven (2004), Implications of the enhanced Brewer-Dobson circulation in European Centre for Medium-Range Weather Forecasts reanalysis ERA-40 for the stratosphere-troposphere exchange of ozone in global chemistry transport models, *J. Geophys. Res.*, *109*, D19308, doi:10.1029/2004JD004586.

Voulgarakis, A., P. J. Telford, A. M. Aghedo, P. Braesicke, G. Faluvegi, N. L. Abraham, K. W. Bowman, J. A. Pyle, and D. T. Shindell (2011), Global multi-year $O_3$-CO correlation patterns from models and TES satellite observations, *Atmos. Chem. Phys.*, *11*, 5819–5838, doi:10.5194/acp-11-5819-2011.

Warner, J. X., M. McCourt Comer, C. D. Barnet, W. W. McMillan, W. Wolf, E. Maddy, and G. Sachse (2007), A comparison of satellite tropospheric carbon monoxide measurements from AIRS and MOPITT during INTEX-A, *J. Geophys. Res.*, *112*, D12S17, doi:10.1029/2006JD007925.

Warner, J. X., Z. Wei, L. L. Strow, C. D. Barnet, L. C. Sparling, G. Diskin, and G. Sachse (2010), Improved agreement of AIRS tropospheric carbon monoxide products with other EOS sensors using optimal estimation retrievals, *Atmos. Chem. Phys.*, *10*, 9521–9533, doi:10.5194/acp-10-9521-2010.

Wei, J. C., et al. (2010), Ozone profile retrieval from an advanced infrared sounder: Experiments with tropopause-based climatology and optimal estimation approach, *J. Atmos. Oceanic Technol.*, *27*, 1123–1139, doi:10.1175/2010JTECHA1384.1.

Weiss-Penzias, P., et al. (2007), Quantifying Asian and biomass burning sources of mercury using the Hg/CO ratio in pollution plumes observed at the Mount Bachelor Observatory, *Atmos. Environ.*, *41*(21), 4366–4379, doi:10.1016/j.atmosenv.2007.01.058.

Wiedinmyer, C., S. K. Akagi, R. J. Yokelson, L. K. Emmons, J. A. Al-Saadi, J. J. Orlando, and A. J. Soja (2011), The Fire INventory from NCAR (FINN): A high resolution global model to estimate the emissions from open burning, *Geosci. Model Dev.*, *4*, 625–641, doi:10.5194/gmd-4-625-2011.

Wimmers, A. J., J. L. Moody, E. V. Browell, J. W. Hair, W. B. Grant, C. F. Butler, M. A. Fenn, C. C. Schmidt, J. Li, and B. A. Ridley (2003), Signatures of tropopause folding in satellite imagery, *J. Geophys. Res.*, *108*(D4), 8360, doi:10.1029/2001JD001358.

Wu, S., B. N. Duncan, D. J. Jacob, A. M. Fiore, and O. Wild (2009), Chemical nonlinearities in relating intercontinental ozone pollution to anthropogenic emissions, *Geophys. Res. Lett.*, *36*, L05806, doi:10.1029/2008GL036607.

Yienger, J. J., M. Galanter, T. A. Holloway, M. J. Phadnis, S. K. Guttikunda, G. R. Carmichael, W. J. Moxim, and H. Levy II (2000), The episodic nature of air pollution transport from Asia to North America, *J. Geophys. Res.*, *105*(D22), 26,931–26,945, doi:10.1029/2000JD900309.

Zhang, L., et al. (2006), Ozone-CO correlations determined by the TES satellite instrument in continental outflow regions, *Geophys. Res. Lett.*, *33*, L18804, doi:10.1029/2006GL026399.

Zhang, L., et al. (2008), Transpacific transport of ozone pollution and the effect of recent Asian emission increases on air quality in North America: An integrated analysis using satellite, aircraft, ozonesonde, and surface observations, *Atmos. Chem. Phys.*, *8*, 6117–6136, doi:10.5194/acp-8-6117-2008.

Zhang, L., D. J. Jacob, M. Kopacz, D. K. Henze, K. Singh, and D. A. Jaffe (2009), Intercontinental source attribution of ozone pollution at western U.S. sites using an adjoint method, *Geophys. Res. Lett.*, *36*, L11810, doi:10.1029/2009GL037950.

Zhang, L., et al. (2011), Improved estimate of the policy-relevant background ozone in the United States using the GEOS-Chem global model with 1/2° × 2/3° horizontal resolution over North America, *Atmos. Environ.*, *45*, 6769–6776, doi:10.1016/j.atmosenv.2011.07.054.

Zhang, Q., et al. (2009), Asian emissions in 2006 for the NASA INTEX-B mission, *Atmos. Chem. Phys.*, *9*, 5131–5153, doi:10.5194/acp-9-5131-2009.

O. R. Cooper, J. Holloway, B. J. Johnson, A. M. Middlebrook, I. B. Pollack, and T. B. Ryerson, NOAA Earth System Research Laboratory, 325 Broadway, Boulder, CO 80305, USA.

A. M. Fiore, Lamont-Doherty Earth Observatory, Columbia University, PO Box 1000, 61 Rte. 9W, Palisades, NY 10964, USA.

L. W. Horowitz, V. Naik, J. Wilson, and B. Wyman, NOAA Geophysical Fluid Dynamics Laboratory, 201 Forrestal Rd., PO Box 308, Princeton, NJ 08540, USA.

M. Lin, Atmospheric and Oceanic Sciences, Princeton University, 201 Forrestal Rd., Princeton, NJ 08540, USA. (meiyunl@princeton.edu)

S. J. Oltmans, Cooperative Institute for Research in Environmental Sciences, University of Colorado at Boulder, Boulder, CO 80309, USA.

J. X. Warner, Joint Center for Earth Systems Technology, University of Maryland, Baltimore County, 5523 Research Park Dr., Ste. 320, Baltimore, MD 21228, USA.

C. Wiedinmyer, National Center for Atmospheric Research, PO Box 3000, Boulder, CO 80307, USA.